

H $\alpha$  TAIL, INTRACLUSTER HII REGIONS AND STAR-FORMATION: ESO 137-001 IN ABELL 3627

M. SUN, M. DONAHUE, G. M. VOIT

Department of Physics and Astronomy, MSU, East Lansing, MI 48824; sunm@pa.msu.edu

Draft version July 26, 2021

## ABSTRACT

We present the discovery of a 40 kpc H $\alpha$  tail and at least 29 emission-line objects downstream of a star-forming galaxy ESO 137-001 in the rich, nearby cluster A3627. The galaxy is known to possess a dramatic 70 kpc X-ray tail. The detected H $\alpha$  tail coincides positionally with the X-ray tail. The H $\alpha$  emission in the galaxy is sharply truncated on the front and the sides near the nucleus, indicating significant ram pressure stripping. ESO 137-001 is thus the first cluster late-type galaxy known unambiguously with both an X-ray tail and an H $\alpha$  tail. The emission-line objects are all distributed downstream of the galaxy, with projected distance up to 39 kpc from the galaxy. From the analysis on the H $\alpha_{\text{off}}$  frame and the estimate of the background emission-line objects, we conclude that it is very likely all 29 emission-line objects are HII regions in A3627. The high surface number density and luminosities of these HII regions (up to  $10^{40}$  ergs s $^{-1}$ ) dwarf the previously known examples of isolated HII regions in clusters. We suggest that star formation may proceed in the stripped ISM, in both the galactic halo and intracluster space. The total mass of formed stars in the stripped ISM of ESO 137-001 may approach several times  $10^7 M_{\odot}$ . Therefore, stripping of the ISM not only contributes to the ICM, but also adds to the intracluster stellar light through subsequent star formation. The data also imply that ESO 137-001 is in an active stage of transformation, accompanied by the build-up of a central bulge and depletion of the ISM.

*Subject headings:* galaxies: ISM — H II regions — galaxies: evolution — stars: formation — galaxies: clusters: individual (A3627) — galaxies: individual (ESO 137-001)

## 1. INTRODUCTION

The intracluster medium (ICM) has long been thought to play a vital role in galaxy evolution in clusters (Gunn & Gott 1972). Ram pressure and turbulence/viscous stripping by the ICM can efficiently remove cold galactic gas and may be responsible for transforming disk galaxies with active star formation into red S0 galaxies (e.g., Quilis et al. 2000). Stripping of the galactic ISM in clusters has been extensively examined in simulations (e.g., Schulz & Struck 2001, SS01 hereafter; Roediger & Hensler 2005, RH05 hereafter), which show that stripping has significant impacts on the properties of galaxies. In the process of stripping, the galactic ISM is removed from the disk and the outer galactic disk is truncated, while the inner disc is compressed, accompanied by formation of numerous flocculent arms (SS01; RH05). The galactic SFR is also modified. Compression of disk ISM may trigger prodigious star formation (e.g., SS01; Bekki & Couch 2003; RH05) in the first  $\sim 10^8$  yr of interaction, even though star formation activity will eventually be suppressed as the galactic ISM is depleted. This initial starburst may explain the blue “Butcher-Oemler galaxies” in  $z \gtrsim 0.3$  clusters (Butcher & Oemler 1978). The further evolution of the stripped ISM from the disk is not clear because of uncertainties in the transport coefficients (conductivity and viscosity). It has been suggested that some stripped ISM may be able to cool to form stars because the main ISM heating source, stellar UV radiation, is much weaker in intracluster space (e.g., SS01). Therefore, ISM stripping in clusters is important for both galaxy evolution and star formation in clusters.

Observational evidence of stripping in cluster late-type galaxies has only begun to accumulate in recent years. Tails behind late-type galaxies have been observed in HI, H $\alpha$  and X-rays (e.g., Gavazzi et al. 2001; Wang et al. 2004; Oosterloo & van Gorkom 2005; Sun & Vikhlinin 2005; Yagi et al. 2007). Recently we found a long X-ray tail in a rich cluster A3627, associated with a late-type galaxy ESO 137-001 (Sun

et al. 2006, S06 hereafter). The narrowness and length of the tail make it the most dramatic X-ray tail of a late-type galaxy to date. It is also the only known X-ray tail from a late-type galaxy in a rich cluster. There are only two other known X-ray tails of late-type galaxies in clusters (C153 in A2125, Wang et al. 2004; UGC 6697 in A1367, Sun & Vikhlinin 2005). Both are in  $\sim 3$  keV clusters that are more distant than A3627 (note  $z = 0.253$  for A2125). We have also examined all *Chandra* and *XMM-Newton* data for  $T > 3$  keV clusters at  $z < 0.1$  (62 clusters in total; for the work on a subsample at  $z < 0.05$ , see Sun et al. 2007). No other significant stripped tails of late-type galaxies have been detected, which implies that ESO 137-001’s current stage is of short duration.

A3627 is a nearby rich cluster ( $z=0.01625$ ,  $\sigma_{\text{radial}} = 925$  km/s and  $kT=6$  keV) rivaling Coma and Perseus in mass and galaxy content (Kraan-Korteweg et al. 1996; Woudt et al. 2007). ESO 137-001 is a blue emission-line galaxy (Woudt et al. 2004) that is only  $\sim 200$  kpc from the cluster’s X-ray peak on the plane of the sky. Its radial velocity ( $4630$  km s $^{-1}$ ) is close to that of A3627 ( $4871 \pm 54$  km s $^{-1}$ , Woudt et al. 2007). S06 found a long narrow X-ray tail behind ESO 137-001, in both *Chandra* and *XMM-Newton* data (also shown in Fig. 1). The tail extends to at least 70 kpc from the galaxy with a length-to-width ratio of  $\sim 10$ . The X-ray tail is luminous ( $\sim 10^{41}$  ergs s $^{-1}$ ), with an X-ray gas mass of  $\sim 10^9 M_{\odot}$ . S06 interpret the tail as the stripped ISM of ESO 137-001 mixed with the hot ICM, while this blue galaxy is being converted into a gas-poor galaxy. The *Chandra* data also reveal three hard X-ray point sources ( $L_X \sim 10^{40}$  ergs s $^{-1}$ ) along the tail (Fig. 1), and the possibility of all of them being background AGN is  $< 0.1\%$ . Thus, we suggested that some of them may be ultra-luminous X-ray sources (ULXs) born from active star formation in the tail. Nevertheless, the optical properties of this interesting galaxy are poorly known in the literature (e.g., Woudt et al. 2004; 2007). In this paper, we present the results from our H $\alpha$  and optical broad-band imaging observations of ESO 137-

001 with SOAR, and spectroscopic observations with the CTIO 1.5m telescope. We adopt a cluster redshift of 0.01625 for A3627 (Woudt et al. 2007), which is a little larger than what we used in S06 (0.0157 from Kraan-Korteweg et al. 1996). Assuming  $H_0 = 73 \text{ km s}^{-1} \text{ Mpc}^{-1}$ ,  $\Omega_M=0.24$ , and  $\Omega_\Lambda=0.76$ , the luminosity distance is 67.6 Mpc, and  $1''=0.317 \text{ kpc}$ .

## 2. OBSERVATIONS AND DATA REDUCTION

### 2.1. SOAR observations

ESO 137-001 was observed with the 4.1 m Southern Observatory for Astrophysical Research (SOAR) telescope on Cerro Pachon on Aug. 28, 2006 (UT) and Mar. 15, 2007 (UT). Both nights were clear and photometric. The observations were made with the SOAR Optical Imager (SOI), which covers a  $5.26'$  square field of view with two CCDs ( $2.6'$  width each, separated by an  $8.1''$  gap). In the 2006 run ( $\sim 0.7''$  seeing, 1.23 - 1.31 airmass), two 20-minute exposures were collected with the  $H\alpha$  filter and five 20-second exposures were taken in the  $I$  band. However, the telescope guider happened to be south of the galaxy in two  $H\alpha$  exposures, blocking any emission  $26''$  south of the galactic nucleus. In the 2007 run ( $\sim 0.9''$  seeing, 1.17 - 1.29 airmass), we took four 20-minute exposures in the  $H\alpha$  band, two 10-minute exposures in another narrow band close to the  $H\alpha$  band (we call it the  $H\alpha_{\text{off}}$  band hereafter), seven 90-second exposures in the  $B$  band and four 30-second exposures in the  $I$  band. The  $H\alpha$  filter used is the CTIO filter ID 6649-76 ( $\lambda_{\text{cen}} = 6650 \text{ \AA}$ , FWHM= $77 \text{ \AA}$ ) as the redshifted  $H\alpha$  line of ESO 137-001 is centered at  $6664 \text{ \AA}$ . The  $H\alpha_{\text{off}}$  filter used is the CTIO filter ID 6520-76 ( $\lambda_{\text{cen}} = 6530 \text{ \AA}$ , FWHM= $71 \text{ \AA}$ ). The bandwidths of the two narrow-band filters overlap little (at  $6590 \text{ \AA}$ , the transmission of the 6649-76 filter is 4.8%, while that of the 6520-76 filter is 2.6%). Both narrow-band filters are 2 inches  $\times$  2 inches, so the non-vignetted field is only  $\sim 3.6' \times 3.5'$ . Dithers of  $15'' - 30''$  were made between exposures. During the second half of 2006, the triplet lens of the focal reducer in SOI became partially unbounded, which caused the photometry to be uncertain to  $\sim 0.2 \text{ mag}$  from the field center to the corners. The lens of SOI was repaired in the beginning of 2007 so the photometry accuracy was recovered before our 2007 run. In this work, we use only the 2007 data in the analysis. Nevertheless, we examined the emission-line objects (see the definition and discussion in §3) in the 2006 data (which had better seeing). All 29 emission-line objects selected from the 2007 data (§3) are confirmed in the 2006 data, although several of them are close to the guider in the 2006 data so their fluxes are reduced.

Each image was reduced using the standard procedures with the IRAF MSCRED package. The pixels were binned  $2 \times 2$ , for a scale of  $0.154''$  per pixel. The fringing on the  $I$  band images was subtracted with the standard fringe frames. Dome flats were used. The US Naval Observatory (USNO) A2.0 catalog was used for the WCS alignment, which was done with WCSTools. Spectrophotometric standards are LTT 4364 and EG 274 (Hamuy et al. 1994). Ten standard stars in two fields (PG 1047 and RU 149) on the  $B$ ,  $V$ ,  $R$  and  $I$  bands were also observed at airmass of 1.1 - 1.8. ESO 137-001 is near the Galactic plane ( $l=325.25 \text{ deg}$ ,  $b=-6.97 \text{ deg}$ ) so the Galactic extinction is substantial. The Galactic extinction at the  $B$ ,  $I$ ,  $H\alpha$  and  $H\alpha_{\text{off}}$  bands is 0.89 mag, 0.40 mag, 0.554 mag and 0.568 mag respectively, derived from the Galactic extinction law by Cardelli, Clayton & Mathis (1989) for  $E(B-V) = 0.207 \text{ mag}$  (from NED). As ESO 137-001 is not far from the Galactic cen-

ter, the uncertainties of Galactic extinction may not be small, but our conclusions of this paper are hardly affected.

### 2.2. CTIO spectroscopic observations

Spectroscopic observations of ESO 137-001 were conducted with the R-C spectrograph on the 1.5m telescope in CTIO, operated by the Small and Moderate Aperture Research Telescope System (SMARTS) Consortium. Two service observations were made on June 20 and 21, 2007, with the 47/Ib and 26/Ia grating setups respectively. The 26/Ia setup covers a wavelength range of  $3660 - 5440 \text{ \AA}$  with a dispersion of  $1.5 \text{ \AA}$  per pixel. The spectral resolution is  $\sim 4.3 \text{ \AA}$ . The 47/Ib setup covers a wavelength range of  $5652 - 6972 \text{ \AA}$  with a dispersion of  $1.1 \text{ \AA}$  per pixel. The spectral resolution is  $\sim 3.1 \text{ \AA}$ . The slit is always aligned east-west with a length of  $\sim 5'$  and a width of  $3''$ . The pixel scale on the CCD is  $1.3''$  per pixel and the best instrumental spatial seeing for the R-C spectrograph is only  $\sim 3.5''$ . For the 26/Ia observation (1.22-1.37 airmass), the slit was set across ESO 137-001's center. Five exposures (20 minutes each) were made in the 26/Ia run and we combined them. The 47/Ib run on June 20, 2007 (1.60-1.91 airmass) was composed of three exposures (25 minutes each). The slit was moved by several arcsec in the north-south direction between exposures by mistake, although it was requested in a fixed position the same as the one for the 26/Ia observations. Thus, we analyzed the three exposures separately. The pattern of the stellar spectra on the CCD (through the long slit) allows us to recover the slit positions. Spectroscopic standards were observed at each night, LTT 4364 for the 26/Ia run and Feige 110 for the 47/Ib run. As these observations of the standards used a  $2''$  slit, absolute flux calibration is impossible, but the analysis of the emission line ratios should not be affected.

## 3. EMISSION-LINE OBJECTS

### 3.1. Selection of emission-line objects

With data in two narrow bands ( $H\alpha$  and  $H\alpha_{\text{off}}$ ) and two broad bands ( $B$  and  $I$ ), we derived color-color and color-magnitude relations for sources in the field covered by all data ( $3.42' \times 3.88'$  around ESO 137-001 shown as the dotted box in Fig. 1b). SExtractor 2.5.0 was used to measure photometry and color. The  $H\alpha$  and  $H\alpha_{\text{off}}$  magnitudes are AB magnitudes defined in Hamuy et al. (1994) and are calibrated with the data of EG 274 and LTT 4364. Galactic extinction has been corrected in all bands. In the  $H\alpha - H\alpha_{\text{off}}$  vs.  $H\alpha - I$  map (Fig. 2), over 97% of 1708 sources in the field are Galactic stars with little excess or decrement emission in the  $H\alpha$  filter. The  $H\alpha - H\alpha_{\text{off}}$  histogram peaks at  $\sim -0.02 \text{ mag}$  and the typical  $1 \sigma$  dispersion is  $\sim 0.15 \text{ mag}$ . The  $H\alpha - I$  histogram peaks at  $\sim 0.46 \text{ mag}$  and is skewed to higher color values. The  $1 \sigma$  dispersion on the lower color side is  $\sim 0.22 \text{ mag}$ . Besides these stars, there are about 30 sources that are especially bright in the  $H\alpha$  band and occupy a different region in the color - color map. In this work, we selected 29 emission-line objects with the following conservative criteria:  $H\alpha - H\alpha_{\text{off}} < -0.7 \text{ mag}$  and  $H\alpha - I < -0.2 \text{ mag}$ . These emission-line objects have equivalent widths (EW) of  $84 - 758 \text{ \AA}$  (we adopted the definition of EW in Gavazzi et al. 2006). Their positions, as shown in Fig. 1b, are all downstream of the galaxy and in or around the X-ray tail. If we relax the criteria to  $H\alpha - H\alpha_{\text{off}} < -0.5 \text{ mag}$  and  $H\alpha - I < 0.25 \text{ mag}$ , six additional sources are selected and they are also in or around the X-ray tail (Fig. 1b).

The  $H\alpha$  mag vs.  $H\alpha - I$  relation is also shown in Fig. 2. After correcting the atmospheric and Galactic extinction, the fluxes of these emission-line objects range from  $1.5 \times 10^{-16} - 4.0 \times 10^{-14}$  ergs  $s^{-1}$   $cm^{-2}$  (no correction for intrinsic extinction). We also derived the  $B - I$  color for sources in the field. As some emission-line objects are not detected in the  $B$  and  $I$  bands,  $B - I$  color can be constrained only for 17 emission-line objects (Fig. 2). The emission-line objects are generally bluer than the galaxy (without correction for intrinsic extinction) and Galactic stars. The  $B - I$  colors of Galactic stars span from M type (3.6 - 5.1 mag) to A type (0 - 0.4 mag). As the Galactic reddening (0.49 mag) was applied on all sources, the actual separation between  $B - I$  colors of emission-line objects and Galactic stars will be wider if zero or smaller Galactic extinction applies on stars and some amount of intrinsic extinction is applied for emission-line objects. Therefore, these emission-line objects are blue and a small amount of intrinsic extinction can drive their colors to those of pure O/B star clusters.

### 3.2. What are they?

What is the nature of these emission-line objects? They cannot be Galactic  $H\alpha$  emitters as the required velocity (2600 km/s - 5300 km/s) is too high. The other emission line close to the  $H\alpha$  filter band is [SII] 6716Å (but generally with small EW). However, a velocity of  $< -1600$  km/s is required to put the [SII] line in the  $H\alpha$  filter band, which is also too large for Galactic objects. Thus, these emission-line objects are extragalactic. Besides being  $H\alpha$  emitters in A3627, these objects could also be [OIII]  $\lambda 5007$  emitters at  $z \sim 0.33$ ,  $H\beta$  emitters at  $z \sim 0.37$ , [OII]  $\lambda 3727$  emitters at  $z \sim 0.78$  and  $Ly\alpha$  emitters at  $z \sim 4.47$ . We have examined the expected number density of these background objects in the following two ways.

First, we can examine the  $H\alpha_{\text{off}}$  frame in the same way as we did for the  $H\alpha$  frame to select emission-line objects in the  $H\alpha_{\text{off}}$  band (or sources with large  $H\alpha - H\alpha_{\text{off}}$  color). Both narrow-band filters have very similar transmission and band width. The difference in their central wavelength is small. Thus, we expect that the number of background emission-line objects detected in the two narrow bands should be similar.  $H\alpha_{\text{off}}$  -  $H\alpha$  vs.  $H\alpha_{\text{off}} - I$  and  $H\alpha_{\text{off}}$  vs.  $H\alpha_{\text{off}} - I$  maps (shown in Fig. 2) are derived for sources detected in the  $H\alpha_{\text{off}}$  band. The same criteria used to select emission-line objects in the  $H\alpha$  band were applied (with just the change from  $H\alpha$  magnitude to  $H\alpha_{\text{off}}$  magnitude). No emission-line objects have been found in the  $H\alpha_{\text{off}}$  band, even though the loose criteria are applied ( $H\alpha_{\text{off}} - H\alpha < -0.5$  mag and  $H\alpha_{\text{off}} - I < 0.25$  mag). In fact, the  $H\alpha_{\text{off}}$  exposure is deep enough to detect the faintest emission-line object in the  $H\alpha$  band, if a similar object is present in the  $H\alpha_{\text{off}}$  frame. This single self-test already demonstrates that the expected number of background emission-line objects is very small.

Second, we examined the number density of emission-line objects from the Large Area  $Ly\alpha$  survey at  $z \sim 4.5$  (Malhotra & Rhoads 2002) as they used the narrow-band filters with similar central wavelength and bandwidth ( $\sim 80\text{\AA}$ ) to ours. Their covered field is  $0.72$  deg<sup>2</sup> and the achieved sensitivity is about 5 times deeper than ours. In three non-overlapping  $H\alpha$  filters (the central one has the same central wavelength as our  $H\alpha$  filter), 157  $Ly\alpha$  candidates (with  $EW > 80\text{\AA}$  and without  $B$  band detection) were detected. The size of our field is  $3.42' \times 3.88'$ . Thus, the expected number of emission-line objects selected in Malhotra & Rhoads (2002) is  $\sim 0.02$  in our field (adjusted to our flux limit by assuming a power index of -1.6 for the lu-

minosity function, Malhotra & Rhoads 2002). Cortese et al. (2004) examined  $\sim 2.5$  deg<sup>2</sup>  $H\alpha$  frames of the Virgo cluster ( $\lambda_{\text{cen}} = 6574 \text{\AA}$ ,  $\Delta\lambda = 95 \text{\AA}$ ) obtained at the Isaac Newton Telescope. Six emission-line objects were detected (for a  $H\alpha$  flux limit of about 6 times shallower than the faintest emission-line object in our sample) and their follow-up spectroscopic observations showed that five of them were [OIII]  $\lambda 5007$  emitters at  $z \sim 0.31$ . If we take their number as the number density of  $z \sim 0.33$  [OIII]  $\lambda 5007$  emitters in the high luminosity and apply a luminosity function with a power index of -1.4 (e.g., Pascual et al. 2001), the expected number of [OIII] emitters in our whole field is  $\sim 0.09$ . For our line flux limit ( $\gtrsim 10^{16}$  ergs  $s^{-1}$   $cm^{-2}$ ), the combined number density of the  $H\beta$  and the [OII]  $\lambda 3727$  emitters is at most comparable to that of [OIII]  $\lambda 5007$  emitters (e.g., Pascual et al. 2001), and these two lines generally don't have high EW.

Therefore, the expected number of background emission-line sources is much smaller than one in our  $3.42' \times 3.88'$  field and it is very likely that *all 29 emission-line objects are  $H\alpha$  emitters associated with A3627*. In fact, this conclusion is even much stronger when we consider the spatial concentration of emission-line objects immediately downstream of ESO 137-001 and around the X-ray tail. *These 29 + 6 sources are not randomly distributed in the field and relative to the galaxy*. Twenty-five emission-line objects cluster in a  $40'' \times 60''$  box region immediately downstream of ESO 137-001, while the area of our total field is 20 times larger. In §4.1, we further show that seven emission-line objects are caught in one or more CTIO 1.5m slit spectra. The spectra strongly support the argument of HII regions (§4.1), at least for these seven emission-line objects. As  $H\alpha$  emitters in A3627, they are too luminous to be intracluster planetary nebulae. The  $H\alpha$  luminosity of the faintest emission-line object in our sample is  $> 7.2$  times larger (without intrinsic extinction) than the [OIII]  $\lambda 5007$  luminosity of the most luminous intracluster planetary nebulae in the Virgo cluster (Ciardullo et al. 1998) and the  $H\alpha$  line of a planetary nebula is generally several times fainter than the [OIII] line. Thus, we conclude that they are HII regions most likely associated with ESO 137-001 and its tail in A3627. Hereafter, we simply refer these emission-line objects as HII regions.

### 3.3. Properties of the HII regions

The properties of these HII regions and the embedded star clusters can be estimated. The intrinsic extinction is unknown. Gerhard et al. (2002) and Cortese et al. (2004) measured  $\sim 1$  mag intrinsic extinction for two isolated HII regions in the Virgo cluster. We simply adopt this value for all HII regions. The [NII]  $\lambda 6548$  and  $\lambda 6584$  lines are in the  $H\alpha$  filter band. The [NII]  $\lambda 6584$  line is close to the wing (transmission there is 65% of the value in the center). Gerhard et al. (2002) and Cortese et al. (2004) measured  $H\alpha / (H\alpha + [\text{NII}] \lambda 6548 + [\text{NII}] \lambda 6584) \sim 0.81$  for two isolated HII regions in the Virgo cluster. This fraction is assumed in our analysis. The derived  $H\alpha$  luminosities of these HII regions are plotted in Fig. 3 versus their distance to ESO 137-001's nucleus. The cumulative luminosity function of these HII regions,  $N(> \log L) \propto L^{-\alpha}$ , has a slope of  $0.6 \pm 0.1$  at  $L_{H\alpha} > 10^{38.3}$  ergs  $s^{-1}$ . With the scaling relation derived by Kennicutt (1998),  $\text{SFR} (M_{\odot}/\text{yr}) = L_{H\alpha} / (1.26 \times 10^{41} \text{ ergs } s^{-1})$ , the SFR in these HII regions ranges from 0.0008 to 0.17  $M_{\odot}/\text{yr}$ , with a total SFR of 0.59  $M_{\odot}/\text{yr}$  for 29 HII regions selected. Assuming an electron temperature of  $10^4$  K and case B of nebular theory, the number of ionizing photons  $Q(\text{H})$  ranges

from  $9.5 \times 10^{49}$  to  $2.1 \times 10^{52} \text{ s}^{-1}$ .

We can apply the Starburst99 model (Leitherer et al. 1999) to estimate the age and the total mass of the starbursts in these HII regions. The age of the starburst can be estimated from the ratio  $Q(\text{H}) / L_B$ , or the ratio  $Q(\text{H}) / L_I$  (e.g., Gerhard et al. 2002), or the  $\text{H}\alpha$  equivalent width — EW ( $\text{H}\alpha$ ). The first two estimates may only provide lower limits on the age as the intrinsic extinction of the HII regions in the  $B$  and  $I$  bands is unknown. EW ( $\text{H}\alpha$ ) is not affected by intrinsic extinction, although the uncertainties are generally large and there are only lower limits in many cases. We selected eight representative HII regions (marked ELO1 to 8 in Fig. 1c and 1d) to demonstrate the range of the properties of these 29 objects. ELO1 is the brightest and the only resolved one (with a radius of  $\sim 0.6$  kpc). ELO2 and 3 are the next two most luminous ones. ELO4 is the one with the lowest EW ( $\text{H}\alpha$ ). ELO5 is only  $\sim 0.4''$  offset from the brightest *Chandra* hard X-ray point source in the tail (P1 in S06). ELO6 is the faintest emission-line object, while ELO7 and 8 are most distant from ESO 137-001’s nucleus in projection (30 - 39 kpc). A metallicity of 0.4 solar is assumed, which is similar to those of two HII regions studied by Gerhard et al. (2002) and Cortese et al. (2004). We assume instantaneous star formation with a Salpeter IMF,  $M_{\text{up}} = 100M_{\odot}$  and  $M_{\text{low}} = 1M_{\odot}$ . The results are listed in Table 1. The age estimated from  $Q(\text{H}) / L_B$  is always the smallest, which implies intrinsic extinction in HII regions. The age is always less than  $\sim 7$  Myr, which is typical for bright HII regions (e.g., Gerhard et al. 2002; Mendes de Oliveira et al. 2004). The estimated age from EW ( $\text{H}\alpha$ ) is not sensitive to the assumed metallicity for EW ( $\text{H}\alpha$ )  $> 400 \text{ \AA}$  HII regions. Even for low EW ( $\text{H}\alpha$ ) regions, the uncertainty of age is not very big. For example, the predicted age of ELO4 from EW ( $\text{H}\alpha$ ) is 6.7, 6.3, 6.5, 8.3, and 11.5 Myr for assumed metallicity of 2, 1, 0.4, 0.2, 0.05 solar respectively. It is clear that these HII regions are all young ( $\lesssim 10$  Myr). The derived total mass ( $\sim 10^3 M_{\odot}$  —  $\sim 4 \times 10^6 M_{\odot}$ ) is sensitive to the age of the starburst, as shown for two HII regions with similar  $\text{H}\alpha$  luminosities (ELO6 and 8, Table 1). The older the HII region is, the more massive it is. Nevertheless, the brightest 5 - 10 HII regions host star clusters with total mass of  $> 10^5 M_{\odot}$ , or super star clusters ( $10^5 - 10^8 M_{\odot}$ , O’Connell 2004). The total mass in the 29 putative HII regions is about  $10^7 M_{\odot}$ , with at least a factor of four uncertainty because of the unknown extinction and uncertain age.

The  $\text{H}\alpha$  emission of HII regions fades rapidly for a single starburst and will be much fainter after the initial 10 Myr. The radial velocity difference between ESO 137-001 and A3627 is only 214 km/s, which implies that ESO 137-001’s infalling is almost in the plane of the sky. If we assume a velocity of ESO 137-001 equal to the velocity dispersion of the cluster (1600 km/s), ESO 137-001 travels only  $\sim 16$  kpc in 10 Myr. It is clear that there are no very luminous HII regions beyond 15 kpc from the nucleus (Fig. 3). We also examined the  $\text{H}\alpha$  EW of the HII regions with offset from the galaxy. There is no clear relation found as 13 sources have only lower limits. Within 8 kpc from the nucleus, the  $\text{H}\alpha$  EW span a big range from 77  $\text{\AA}$  to 614 $\text{\AA}$ . In any case, the three HII regions at 29 - 39 kpc projected from the nucleus must have had star formation happening in the last  $< 10$  Myr, at least 10 - 15 Myr after the gas was removed from ESO 137-001. Thus, the star formation in these HII regions does not always start immediately after they are displaced from the galactic disk, if star formation in these HII regions is indeed a single burst. It is likely that more HII

regions downstream of ESO 137-001 are yet to form and many HII regions may have already faded in or around the tail. We discuss the population of the HII regions more in §6.

#### 4. THE OPTICAL PROPERTIES OF ESO 137-001

##### 4.1. The spectroscopic properties

The spectroscopic properties of the central emission nebula of ESO 137-001 are examined with the CTIO 1.5m spectra. The slit positions are recovered from the stellar spectra on slits, and they are shown in Fig. 4. The #1 slit of the 47/Ib observations misses the central emission nebula of the galaxy. The stellar spectrum at this offset position is too faint to be studied with this single exposure, while a nearby star (close to source “a” in Fig. 4, see also Fig. 1) is several times brighter. The #3 slit of the 47/Ib observations covers the  $\text{H}\alpha$  peak of ESO 137-001 and the resulting spectrum is the brightest. The spectra of ESO 137-001’s central part are shown in Fig. 5, from the combined 26/Ia exposures and the #3 47/Ib exposure. The measured velocity with RVSAO is  $4667 \pm 135$  km/s from the 26/Ia spectrum and  $4640 \pm 20$  km/s from the #3 47/Ib spectrum, which is consistent with  $4630 \pm 58$  km/s measured by Woudt, Kraan-Korteweg & Fairall (1999). As shown in Fig. 5, many line ratios can be determined. However, the 26/Ia and 47/Ib spectra were taken at different nights and at different positions. It is also impossible to do absolute flux calibration for these spectra. Therefore, we restrict our line ratio analysis only to lines in the same wavelength ranges (26/Ia or 47/Ib), which makes the usual method to constrain the intrinsic reddening with the  $\text{H}\alpha / \text{H}\beta$  ratio impossible to be applied. Instead, we use the  $\text{H}\gamma / \text{H}\beta$  ratio to constrain the intrinsic reddening. The theoretical value for pure recombination is taken from Osterbrock (1989), 0.468 for  $10^4$  K gas (case B) at  $n_e = 10^2 \text{ cm}^{-3}$ . The line ratio measured is 0.35, after the correction for the Galactic reddening. Using the Galactic extinction curve from Cardelli et al. (1989) and assuming  $R_V = A_V / E(B - V) = 3.1$ , we derive  $A_V = 1.7$  mag for the intrinsic extinction along ESO 137-001’s core. The corresponding intrinsic extinction for the  $\text{H}\alpha$  line is 1.4 mag, which is consistent with the typical extinction of the  $\text{H}\alpha$  line for nearby spirals (0.5 - 1.8 mag, e.g., Kennicutt 1983) and the likely near edge-on orientation of the galaxy (see §5). Therefore, this amount of intrinsic extinction has been applied to the line ratio analysis in this paper.

The gas properties can be determined with the emission line ratios. We derived various line ratios from the combined 26/Ia spectrum and the #3 47/Ib spectrum as their emission comes from similar regions of the galaxy (Fig. 4). We caution that the flux calibration at the blue end of the spectrum is more vulnerable to the flat field correction so the error of the [OII] flux is bigger than those of other strong emission lines. The [SII]  $\lambda 6716 / [\text{SII}] \lambda 6731$  ratio is  $\sim 1.38$ , which is typical for HII regions and is comparable to the low-density limit of 1.35 (van Zee et al. 1998). The strong [OII] line compared to the [OIII] lines suggests a low ionization parameter of the gas. We derived:  $\log([\text{OI}] \lambda 6300 / \text{H}\alpha) \lesssim -1.65$ ,  $\log([\text{OIII}] \lambda 5007 / [\text{OII}]) = -1.39$ ,  $\log([\text{NII}] \lambda 6584 / \text{H}\alpha) = -0.42$ ,  $\log([\text{SII}] \lambda \lambda 6716, 6731 / \text{H}\alpha) = 0.39$  and  $\log([\text{OIII}] \lambda 5007 / \text{H}\beta) = -0.51$ . All these ratios indicate that the central emission nebula of ESO 137-001 resembles a typical giant HII region (Fig. 4 and 5 of Kewley et al. 2006). The low [OI]  $\lambda 6300 / \text{H}\alpha$  ratio implies that any central AGN, if existed, is very weak, which is consistent with the X-ray non-detection of the nucleus (a  $3\sigma$  limit of  $5 \times 10^{39}$  ergs  $\text{s}^{-1}$  in the 0.5 - 10 keV band).

The gas metallicity can be estimated from several emission line ratios (e.g., Kewley & Dopita 2002), but these line ratios also depend on the ionization parameter. The ionization parameter can be estimated from the [OIII]  $\lambda 5007$  / [OII] ratio, 0.041, which implies an ionization parameter ( $q$ ) of  $\lesssim 10^7$  cm/s for gas metallicity of  $< 2.0$  solar (Kewley & Dopita 2002). We then estimate the gas metallicity from the following line ratios for  $q \lesssim 10^7$  cm/s (Kewley & Dopita 2002):

1.  $\log([\text{NII}] \lambda 6584 / [\text{SII}] \lambda \lambda 6716, 6731) = 0.015$ , which implies  $\log(\text{O}/\text{H})+12 = 8.75 - 8.95$ .
2.  $\log([\text{OII}] \lambda 3727 + [\text{OIII}] \lambda \lambda 4959, 5007 / \text{H}\beta)$  (or  $R_{23}$ ) = 0.90, which implies  $\log(\text{O}/\text{H})+12 = 8.05 - 8.20$  or  $\sim 8.65$ .
3.  $\log([\text{NII}] \lambda 6584 / \text{H}\alpha) = -0.44$ , which implies  $\log(\text{O}/\text{H})+12 \sim 8.73$  or 9.35.
4.  $\log([\text{NII}] \lambda 6584 / [\text{OII}]) = -0.84$ , which implies  $\log(\text{O}/\text{H})+12 = 8.62-8.75$ .

As the line fluxes of [NII] and [OII] come from different observations, their ratio is estimated by multiplying these three line ratios, [NII]  $\lambda 6584 / \text{H}\alpha$ ,  $\text{H}\alpha / \text{H}\beta$  and  $\text{H}\beta / [\text{OII}]$ . For the  $\text{H}\alpha / \text{H}\beta$  ratio, the theoretical value of 2.86 is used for case B recombination at  $10^4$  K and  $n_e \sim 100 \text{ cm}^{-3}$  (Osterbrock 1989). In spite of uncertainties, we find that  $\log(\text{O}/\text{H})+12 \approx 8.7$  (0.6 solar) is consistent with all estimates.

As shown in Fig. 4, seven emission-line objects are also in one or more slit spectra. A large part of ELO1's emission is in the 26/1a spectra. However, the best instrumental spatial seeing for the spectrograph is  $\sim 3.5''$  (or 2.7 pixels). Since both ELO1 and the  $\text{H}\alpha$  core of ESO 137-001 are extended (Fig. 1) and their peaks are only  $4.6''$  away, their lines will be blended in the spectra. Nevertheless, we indeed observe extension of the  $\text{H}\beta$ , [OII]  $\lambda 3727$  and [OIII]  $\lambda 5007$  emission towards the direction of ELO1 (or upward on the CCD plane, Fig. 4). The scale of the extension is consistent with the position of ELO1.

The other six emission-line objects only appear as a single line in each spectrum, because their continua are very weak. Although a single line detection does not determine their redshifts, the following arguments support that at least the bright ones among them are HII regions. First, if we stack all three 2D spectra shown in Fig. 4, we detect significant [NII]  $\lambda \lambda 6548, 6584$  emission at  $\sim 5\sigma$ . Second, the centroids of these lines are only  $< 3\text{\AA}$  (or 137 km/s) higher than the  $\text{H}\alpha$  line of the galaxy. Third, if the detected line is [OIII]  $\lambda 5007$  or  $\text{H}\beta$  at higher redshifts, we expect significant  $\text{H}\beta$  or [OIII] 5007 line also in the 47/1b spectra from the usual [OIII] 5007 /  $\text{H}\beta$  ratio (Kewley et al. 2006). However, they are not detected in either a single exposure or the stacked exposure. Good quality spectra of these emission-line objects would require a big telescope.

#### 4.2. The $\text{H}\alpha$ and broad-band images

The photometric properties of ESO 137-001 are also studied. As shown in Fig. 1, the galaxy may have a distorted inner disk or bar within 1 kpc radius. A dust lane is also significantly detected in all four bands at 0.5 kpc to the south of the nucleus. However, detail around the nucleus can only be obtained with *HST* imaging. The morphological type of ESO 137-001 (e.g., from Sb to Sd) is also unclear. Downstream in the  $B$  and  $I$  band

images, some substructures are detected to  $\sim 6$  kpc from the nucleus, including two blue streams (Fig. 1g). Interestingly, these structures all have nearby emission-line objects. Arm-like features are also detected at the north ( $\sim 35''$  from the nucleus) and the south ( $\sim 26''$  from the nucleus). To quantitatively examine the optical light distribution of ESO 137-001, we measured surface brightness profiles along the minor axis and the major axis (Fig. 6). Although we estimated the intrinsic reddening around the galactic center in §4.1, the intrinsic reddening outside the  $\text{H}\alpha$  emission nebula is unknown and may be smaller. Thus, we elect not to correct for the intrinsic extinction for these profiles. The  $\text{H}\alpha$  emission is very asymmetric along the minor axis because of the HII regions and the  $\text{H}\alpha$  tail downstream of the galaxy. The net  $\text{H}\alpha$  emission is truncated sharply upstream at  $\sim 0.9$  kpc from the nucleus. The  $\text{H}\alpha$  emission is much more symmetric along the major axis, and the net  $\text{H}\alpha$  emission is truncated sharply at  $\sim 1.5$  kpc from the nucleus. In the optical, the galaxy is composed of at least two components (Fig. 6). The bright inner component extends to  $\sim 1.9$  kpc in radius along the major axis and to  $\sim 1.2$  kpc in radius along the minor axis. Almost all  $\text{H}\alpha$  emission is within the inner component. Within the central 1.5 kpc radius, the  $B$  and  $I$  band light distributions have multiple peaks. The outer component can be fitted with an exponential profile and the derived scale height is  $\sim 6''$  along the minor axis and  $\sim 12''$  along the major axis (see the caption of Fig. 6). The light distribution is a little more extended in the north, compared to that in the south (Fig. 6).

We also measured the light profiles in elliptical annuli centered on the  $\text{H}\alpha$  peak (see Fig. 6). Again, the light profiles at  $a = 7'' - 32''$  ( $a$ : the semi-major axis) can be fitted with an exponential profile with a scale height of  $\sim 9.5''$ , while fits with the de Vaucouleurs 1/4 law overestimate the emission at  $a > 25''$ . Although the measured light profiles (without correction on the intrinsic reddening) imply little change of the  $B - I$  color with  $a$ , the known intrinsic reddening in the central  $\text{H}\alpha$  nebula implies that the  $B - I$  color is 1.2 mag bluer there. This blue and bright core may be a central bulge in formation. The orientation of ESO 137-001's disk can be estimated from the classical Hubble formula<sup>1</sup>. Assuming an axis ratio of  $\sim 2$  and a morphological type from Sb to Sd, the estimated angle between the line of sight and the disk plane is 26 - 29 deg. Thus, the putative disk is viewed close to edge-on.

We also derived the total  $B$  and  $I$  band magnitudes of ESO 137-001 with the light profiles derived in elliptical annuli (Fig. 6). The total  $B$  band magnitude measured within a  $20'' \times 40''$  ellipse is  $14.31 \pm 0.08$  mag (or  $\sim 2/3 L_*$  in the  $B$  band), after correcting the atmospheric and Galactic extinction. This value can be compared with the  $B$  magnitude listed on HyperLeda,  $14.05 \pm 0.23$  mag from the ESO survey. Our images are deeper and allow much better masking of Galactic stars as some of them are very close to the nucleus (Fig. 1). The total  $I$  band magnitude measured in the same aperture is  $13.20 \pm 0.07$  mag, after correcting the atmospheric and Galactic extinction. The half-light size of the galaxy is also estimated from the light profiles measured in elliptical annuli:  $14.5''$  (or 4.45 kpc) semi-major axis in the  $B$  band and  $14.0''$  (or 4.30 kpc) semi-major axis in the  $I$  band. The 2MASS  $K_s$  total magnitude is 12.163 mag, after correction for the Galactic extinction (0.076 mag). The intrinsic reddening measured for the  $\text{H}\alpha$  emission nebula would imply a corrected  $B - K_s$  color of  $\sim 0$ , although the real averaged value should be higher as the regions outside of the

<sup>1</sup> <http://leda.univ-lyon1.fr/leda/param/incl.html>

H $\alpha$  emission nebula may have smaller intrinsic extinction. In any case, the  $B - K_s$  color of ESO 137-001 is much bluer than that of a typical late-type galaxy ( $\sim 2 - 3.5$ , Jarrett 2000). The galaxy is way off the red-sequence of galaxies in clusters and is in the so-called “blue cloud” in the cluster color-magnitude relation. The  $K_s$  band absolute magnitude is  $-21.97$  mag. Bell et al. (2003) determined the local  $K_s$  band luminosity function and found an absolute magnitude of  $-23.97$  mag for an  $L^*$  galaxy (with early-type and late-type galaxies mixed, adjusted to the cosmology we used). Therefore, ESO 137-001 is a  $0.16 L^*$  galaxy in the  $K_s$  band. The total stellar mass of ESO 137-001 can also be estimated. The mass-to-light ratios in the  $I$  and  $K_s$  bands can be estimated from the relations derived in Bell & De Jong (2001):  $M/L_I = 0.59 (M/L_I)_\odot$ ,  $M/L_{K_s} = 0.35 (M/L_{K_s})_\odot$  (using the function for the  $K$  band) for  $B - I = 1.1$  mag. The resulting stellar mass of ESO 137-001 is  $4.9 \times 10^9 M_\odot$  from  $L_I$  and  $4.6 \times 10^9 M_\odot$  from  $L_{K_s}$ . The total stellar mass will be smaller if a correction for the intrinsic reddening is made. For example, for an intrinsic reddening of  $0.5$  mag for the  $B - I$  color, the total stellar mass of ESO 137-001 will be one third smaller. Bell et al. (2003) also determined the  $M_*$  of the local stellar mass function,  $M_* = 8.0 \times 10^{10} M_\odot$ . Therefore, though ESO 137-001 is not a small galaxy, it is blue and has a low stellar mass ( $\sim 0.05 M_*$ ).

The net H $\alpha$  emission of ESO 137-001 was also studied. The continuum emission in the H $\alpha$  image is determined from the H $\alpha_{\text{off}}$  frame and the scaling factor was determined to account for all emission of stars in the H $\alpha$  image (or H $\alpha - \text{H}\alpha_{\text{off}} = 0$ , Fig. 2). The net H $\alpha$  image is shown in Fig. 1c and 1d. The net H $\alpha$  flux is also measured. The calibration sources LTT 4364 and EG 274 have nearly flat spectra within the H $\alpha$  filter, while the net narrow-band image of ESO 137-001 is composed of three narrow lines. We can correct for this spectral difference and subtract the [NII] flux with the CTIO spectrum (§4.1) and the transmission curve of the H $\alpha$  filter. The H $\alpha$  and the [NII]  $\lambda\lambda 6548, 6584$  lines can be approximated by three Gaussians with  $\sigma$  of  $\sim 3 \text{ \AA}$ . Their flux ratios are known from the CTIO data. Thus, the conversion factor from the count rate to flux can be derived. The flux is first measured in an elliptical aperture with  $3''$  (semi-minor axis)  $\times 5''$  (semi-major axis) centered on the H $\alpha$  peak (Fig. 6), which encloses almost all emission of the central nebula. The H $\alpha$  EW is  $50 \text{ \AA}$ , which can be compared with the H $\alpha$  EW derived from the CTIO spectra ( $26 \text{ \AA}$  from the slit position #2,  $63 \text{ \AA}$  from the slit position #3). With an intrinsic extinction of  $1.4$  mag (§4.1), the flux is  $2.7 \times 10^{-13} \text{ ergs s}^{-1} \text{ cm}^{-2}$  and the luminosity is  $1.5 \times 10^{41} \text{ ergs s}^{-1}$ . The total H $\alpha$  luminosity of ESO 137-001, measured in a boxy aperture ( $20'' \times 26''$ , shown in Fig. 1d, including HII regions ELO1 and several others), is  $2.5 \times 10^{41} \text{ ergs s}^{-1}$  (still assuming  $1.4$  mag intrinsic extinction). With the scaling relation by Kennicutt (1998), the current SFR in the galaxy is  $\sim 2 M_\odot/\text{yr}$ .

## 5. THE H $\alpha$ TAIL

The H $\alpha$  tail behind ESO 137-001 is significant in the first  $1'$  from the nucleus, even without continuum subtraction (Fig. 1). Nevertheless, the high density of the foreground stars makes the detection of faint, diffuse H $\alpha$  emission not easy in this region. In our analysis, bright stars are masked and the rescaled H $\alpha_{\text{off}}$  image is subtracted. The net H $\alpha$  image shows a tail to at least  $2.2'$  (or  $40 \text{ kpc}$ ) from the galaxy. We notice that the end of the X-ray tail is close to the brightest star in the field, which makes detection of faint, diffuse H $\alpha$  emission very difficult there. The

width of the H $\alpha$  tail ranges from  $3 - 4 \text{ kpc}$ . The H $\alpha$  tail aligns with the X-ray tail very well and both of them are brighter in the first  $1'$  from the nucleus (the “Head” region of the X-ray tail discussed in S06) than in regions beyond.

The total H $\alpha$  flux in the tail is measured in an  $106'' \times 18''$  box covered the whole tail. This box is adjacent to the  $20'' \times 26''$  aperture used in §4.2 to measure the total H $\alpha$  flux in ESO 137-001. Emission-line objects and stars in the tail are masked and the H $\alpha$  fluxes in their positions are recovered from their immediate surroundings. Without correction for intrinsic extinction, the total H $\alpha$  flux in the tail is  $4.4 \times 10^{-14} \text{ ergs s}^{-1} \text{ cm}^{-2}$  and the total luminosity is  $2.4 \times 10^{40} \text{ ergs s}^{-1}$  (with the same conversion factor used for the H $\alpha$  emission of the galaxy in §4.2). The H $\alpha$  surface brightness in the tail ranges from  $7.4 \times 10^{-17} \text{ ergs s}^{-1} \text{ cm}^{-2} \text{ arcsec}^{-2}$  near the galaxy to  $1.6 \times 10^{-17} \text{ ergs s}^{-1} \text{ cm}^{-2} \text{ arcsec}^{-2}$  in the faint region, with an average of  $\sim 2.8 \times 10^{-17} \text{ ergs s}^{-1} \text{ cm}^{-2} \text{ arcsec}^{-2}$ . This average surface brightness is similar to that of D100’s H $\alpha$  tail in Coma cluster ( $0.5 - 4 \times 10^{-17} \text{ ergs s}^{-1} \text{ cm}^{-2} \text{ arcsec}^{-2}$ , Yagi et al. 2007) and  $5 - 10$  times higher than those of H $\alpha$  tails behind two irregular galaxies in A1367 (Gavazzi et al. 2001). In Coma and A1367, the surface density of foreground stars is a lot smaller, which permits detection of faint H $\alpha$  features. We follow Yagi et al. (2007) to estimate the mass of the H $\alpha$  tail. Assuming a cylinder with a  $3.5 \text{ kpc}$  diameter and a  $40 \text{ kpc}$  length (note the tail is somewhat twisted), the rms electron density in the tail is  $\sim 0.045 \text{ cm}^{-3}$ . The total mass is then  $5 \times 10^8 M_\odot$  for a filling factor of unity. This amount of mass for  $10^4 \text{ K}$  gas in the tail is similar to the X-ray gas mass of the tail in the same portion,  $\sim 6 \times 10^8 M_\odot$  from S06. However, both the  $10^4 \text{ K}$  gas and the  $10^7 \text{ K}$  gas in the tail can be very clumpy. If the filling factor for the H $\alpha$  emitting gas is  $0.05$ , the total mass of the H $\alpha$  tail reduces to  $10^8 M_\odot$ . Nevertheless, the stripped ISM in the tail accounts for a significant portion of the original ISM in the galaxy. The tail may also have cooler gas component. ESO 137-001 was undetected in the HI observations with ATCA by Vollmer et al. (2001). However, the limit,  $\sim 10^9 M_\odot$ , is rather high, largely because of the nearby ( $14.5'$  away) bright radio galaxy PKS 1610-60. Future more sensitive radio HI and infrared observations are required to better quantify the ISM content in the galaxy and in the tail.

## 6. DISCUSSION

### 6.1. The formation of HII regions in the halo and the tail

Our observations reveal at least 29 HII regions, all downstream of ESO 137-001. Interestingly, the HII regions closest to the galactic disk form a bow-like front with the axis close to the tail. Their projected distances from the galactic nucleus are up to  $39 \text{ kpc}$ . Most of them (if not all of them) appear away from the galactic disk plane. Similar intracluster HII regions have been found before in the Virgo cluster: one HII region  $21 \text{ kpc}$  from NGC 4388’s nucleus in projection (Gerhard et al. 2002) and one HII region  $3 \text{ kpc}$  off the disk and  $6.5 \text{ kpc}$  from NGC 4402’s nucleus in projection (Cortese et al. 2004). Both galaxies are  $2 - 3.2$  times more luminous than ESO 137-001 in the  $K_s$  band, while their isolated HII regions have H $\alpha$  luminosities of only  $1.3 \times 10^{37} \text{ ergs s}^{-1}$  and  $2.9 \times 10^{38} \text{ ergs s}^{-1}$  respectively (intrinsic extinction corrected). Intergalactic HII regions in poorer environments have also been found (Ryan-Weber et al. 2004; Mendes de Oliveira et al. 2004). However, none of these known examples match the high number density and luminosities of HII regions downstream of ESO 137-001.

For example, 17 HII regions found in this work have  $H\alpha$  luminosities of  $> 3 \times 10^{38}$  ergs  $s^{-1}$  before correction for intrinsic extinction, while only one in previous work (the brightest one in Mendes de Oliveira et al. 2004) is this luminous. Moreover, five HII regions found in this work are up to five times more luminous than the brightest one in Mendes de Oliveira et al. (2004). Thus, the isolated star formation activity downstream of ESO 137-001 is unprecedented.

As ESO 137-001 traverses A3627, its dark matter halo is tidally truncated by the cluster tidal field. As we don't know any characteristic velocity of the galaxy, only a crude estimate can be made. In the simulations by Gnedin (2003), a dark matter halo of a large spiral galaxy with a circular velocity of 250 km/s is truncated at  $30 \pm 6$  kpc in a cluster similar to the Virgo cluster ( $\sigma_{\text{radial}} = 660$  km/s). In smaller galaxies, the truncation radius is proportional to the circular velocity. From the Tully-Fisher relation (e.g., Gnedin et al. 2007), a disk galaxy with ESO 137-001's stellar mass has a typical circular velocity of  $\sim 100$  km/s. Thus, we take a conservative estimate of 15 kpc for the tidal truncation radius of ESO 137-001's dark matter halo. This estimate is also consistent with the analytical estimate by Merritt (1988). As shown in Fig. 1, most HII regions may still be in the halo, although three objects at 29 - 39 kpc from the galaxy in projection are hardly still bound. Without velocity measurements, it is unknown whether most HII regions are still bound in the galactic halo. However, they may easily escape ESO 137-001's potential via weak tidal interaction that barely affects the galactic disk. We also notice that both the  $H\alpha$  and X-ray tails are brightest in the halo.

How did these HII regions form? There is no indication in the optical that ESO 137-001 is merging with another galaxy. ELO1 is an emission-line source with insignificant continuum (Fig. 1 and Table 1). In fact, the merger rate in a massive cluster like A3627 should be very small as the cluster velocity dispersion is high ( $\sigma_{\text{radial}} = 925$  km/s for A3627). Within 100 kpc (or  $5.3'$ ) from the end of the X-ray tail, there are only two other galaxies identified from DSS2, 2MASS and our data, WKK 6166 and another small galaxy without NED ID (G1 and G2 in Fig. 1b). Neither has velocity information in the literature, and both are in the FOV of our SOAR data. In the  $I$  band, WKK 6166 is 1.6 - 1.9 mag fainter than ESO 137-001, depending on whether its center is blended with a star. Its radius is only  $\sim 10''$ , or 3.2 kpc if it is in A3627. The other galaxy (G2 in Fig. 1b) is blended with a star. In the  $I$  band, it is 2.5 - 2.7 mag fainter than ESO 137-001, with a major axis extending to  $\sim 7.5''$ . As both galaxies are redder than ESO 137-001 with  $B - I$  of 1.9 - 2.0 mag, their stellar mass is  $\sim 30\%$  -  $75\%$  of ESO 137-001's, from the mass-to-light ratios in Bell & De Jong (2001). However, even if these two galaxies are in A3627 and have had recent fly-bys with ESO 137-001 to tidally strip the gas clouds responsible for these HII regions, stars should also be tidally stripped. We would expect both stellar trails and the HII regions to be present in both directions from ESO 137-001. On the contrary, the HII regions are present only in a 120 deg cone downstream of ESO 137-001. There are some continuum features downstream of ESO 137-001 up to 6 kpc from the nucleus (Fig. 1 and Fig. 6). However, all of them have bright HII regions within or nearby. The upstream side of the galaxy appears undisturbed and free of any tidal features in both the  $B$  and  $I$  bands.

Cluster galaxies also undergo tidal interaction with the cluster potential (e.g., Gnedin 2003). Recently, Cortese et al.

(2007) reported two peculiar galaxies in the massive clusters A1689 ( $z = 0.18$ ) and A2667 ( $z = 0.23$ ). *HST* images reveal stellar trails composed of bright blue knots and fainter streams behind both galaxies extending to 20 kpc and 75 kpc respectively. The fainter galaxy 131124-012040 in A1689 has a similar NIR luminosity to ESO 137-001, although the star formation in the galaxy has stopped  $\sim 100$  Myr ago. They argue that these features are produced through tidal interaction with the cluster potential. However for ESO 137-001, there are no stellar trails connecting the HII regions, at least in the current data. The detected stellar features 6 kpc downstream of the galaxy are confined around the emission-line regions and hardly extend much. Thus, it is unclear how tidal interactions can strip the clouds responsible for the current HII regions and star clusters, yet not produce stellar trails. Future observations, like optical spectroscopy along both axes and *HST* imaging, will allow us to further quantify the dynamical state of ESO 137-001 (e.g., how dynamically cool is the disk?) and the stellar diffuse emission downstream of the galaxy.

The significance of ram pressure stripping in ESO 137-001 and the bow-like front of the HII region distribution drive us to consider another formation mechanism for these HII regions, star-formation in the ram-pressure displaced ISM clouds. ESO 137-001 is undergoing a strong interaction with the surrounding ICM, judging by the compactness of the remnant  $H\alpha$  disk. Assuming an ambient ICM density of  $6 \times 10^{-4}$   $\text{cm}^{-3}$  and an ICM temperature of 6 keV (see S06), and for a velocity of the galaxy of 1600 km/s ( $\sim \sqrt{3}\sigma_{\text{radial}}$ ), the thermal pressure is  $0.4 \times 10^5$  K  $\text{cm}^{-3}$ , while the ram pressure is  $1.1 \times 10^5$  K  $\text{cm}^{-3}$ . Therefore, the ram pressure is high enough to strip 10 K - 100 K ISM clouds with density up to  $10^4$   $\text{cm}^{-3}$ . HI gas will be stripped, as well as some less dense dark clouds and the outskirts of molecular clouds, even though the dense cores of molecular clouds may remain in the disk plane. Schaye (2004) found a critical surface density of  $N_H = (3 - 10) \times 10^{20}$   $\text{cm}^{-2}$  for star formation in the outer parts of the galactic disks. Some stripped dense clouds from the disk of ESO 137-001 should have higher surface density than this critical value, even if clouds are very clumpy. Thus, the ability of high ram pressure to displace dense clouds from the disk may affect the efficiency of star formation in the stripped ISM. The initial instantaneous stripping can be fast in a high ram pressure environment ( $\gtrsim 10$  Myr from RH05), while most materials stripped off the disk still remain bound. The subsequent evolution of the stripped ISM is complicated. Simulations (Vollmer et al. 2001; SS01; RH05) show that a fraction of stripped materials (mainly from the outer disk,  $\sim 10\%$  from RH05) can still be bound in the galactic halo (the "hang-up" effect) for a few 100 Myr even in a high ram pressure environment. Some material may even fall back to the disk, while most of the stripped ISM concentrates within several galaxy diameters downstream, in the lee of the galaxy where the ram pressure is reduced (e.g., SS01). The details of the process rely on many factors, for example, the porosity of the ISM in the inner disk or the effective ram pressure downstream of the galaxy, the halo potential, and the efficiency of heat conduction and viscosity. Simulations (RH05; Roediger, Brügggen & Hoeft 2006) also show that the wake can be very turbulent. The stripped clouds will collide with each other, which may produce shocks and trigger star formation. Moreover, being in the halo separates them from the strong stellar UV heating flux present in the disk, allowing cooling to be dominant. Thus, star formation may proceed in the halo or



even in unbound clouds far away from the galaxy (e.g., ELO8 and 9). We notice that Oosterloo et al. (2004) reported that two intergalactic HII regions at least 100 kpc from the nearest galaxy (an elliptical) are in a massive isolated HI cloud. HII regions in HI clouds were also reported in Stephan's quintet by Mendes de Oliveira et al. (2004). Thus, star formation in isolated HI clouds is plausible, although the efficiency may be low as suggested by Oosterloo & van Gorkom (2005). This scenario can explain the spatial distribution of the HII regions although the details are certainly complicated. SS01 even suggested formation of dwarf galaxies by these means. We indeed notice that the brightest HII region, ELO1, has an estimated total mass of  $\sim 4 \times 10^6 M_{\odot}$ . If star formation in ELO1 is still active, ELO1 may grow into a dwarf galaxy eventually. Future *HST* and high-resolution HI observations are required to better understand ELO1, other bright HII regions and the stripped ISM.

### 6.2. The fate of the isolated HII regions and their implications

The estimated ages of the HII regions are less than  $\sim 8$  Myr. The length of the X-ray tail implies that stripping has lasted for  $\sim 50$  Myr (assuming a velocity of  $\sim 1500$  km/s in the plane of the sky). Thus, it is possible that many HII regions may have already faded. Nevertheless, the long spatial distribution of the HII regions along the tail implies that after the ISM has been stripped, the time lapse to the beginning of star formation spans a range up to  $\sim 20$  Myr or more (e.g., for ELO8 and 9). Contrary to ELO8 and 9, some luminous HII regions (e.g., ELO1 - ELO3) are only  $\sim 1.6 - 5$  kpc from the galactic disk in projection, but their ages are comparable to those of ELO8 and 9 (if not longer). Their estimated ages are longer than the required time to produce the observed projected offsets. Thus, this may be the evidence that a significant part of stripped ISM from the disk can still be bound in the halo.

We also explore the possibility of detecting faded HII regions from the imaging data. The six additional emission-line regions selected with looser criteria (Fig. 2) are certainly candidates with stronger *I* band continuum. They are also close to the 29 HII regions. The embedded star clusters are blue if the intrinsic extinction is not too high. From Starburst99 model, we find that star clusters like those in ELO1 - 3 should be detected in *B* and *I* bands with our data, even at ages of 50 - 60 Myr. However, it is difficult to distinguish them from the various types of Galactic stars in the foreground. About 10 Myr after the initial starburst, red supergiants appear and the galactic colors are highly metallicity dependent over this period. For star clusters with metallicities larger than 0.4 solar, Starburst99 also predicts a big increase for the *B* - *I* color at  $\sim 10$  Myr for instantaneous starbursts. *B* - *I* color can be as high as 1.7 mag in that period, which makes it almost impossible to select them from Galactic stars with imaging data alone (Fig. 2). In fact, ten non-emission-line objects with *B* - *I* < 0.8 mag (Fig. 2) are mostly bright stars and none of them are close to the tail. Thus, faded HII regions may be selected only through a spectroscopic survey.

If formation of massive stars proceeds in the stripped ISM, high-mass X-ray binaries may form in those star clusters. The existing shallow (14 ks) *Chandra* observation reveals only three hard X-ray point sources in the tail ( $\gtrsim 10^{40}$  ergs s $^{-1}$  if in A3627), but both the XMM-Newton and the *Chandra* spectra reveal an unresolved hard component in the tail (S06). Interestingly, the brightest *Chandra* point source P1 (S06) is only

$\sim 0.4''$  from the putative HII region ELO5 (Fig. 1), while the combined positional uncertainty from *Chandra* and the SOAR data can be up to  $\sim 0.3''$ . The *Chandra* point source P3 positionally coincides with a red optical source (*B* - *I*=3.2) with an  $H\alpha - H\alpha_{\text{off}}$  color of 0.01, which is likely a star. The *Chandra* point source P2 is  $0.7'' - 0.9''$  from two star-like objects, but only  $2.5''$  away from an emission-line object candidate (Fig. 1). We have a 150 ksec *Chandra* ACIS-S observation approved for cycle 9, which can probe the X-ray point source distribution 20 times deeper than the existed data.

The ESO 137-001 data strongly imply a connection between stripping of the ISM and star formation in the halo and intracluster space. The stripped ISM not only contributes to the ICM, but also adds intracluster light by subsequent star formation after stripping. The total mass of starbursts in the 29 HII regions is about  $10^7 M_{\odot}$  (with large uncertainty from age and extinction), while the total gas mass of the  $H\alpha$  tail and the X-ray tail is  $\lesssim 10^9 M_{\odot}$  (depending on the filling factor and density variation). As many HII regions may have already faded and star formation may still proceed in the stripped ISM, the final total stellar mass formed in the halo and intracluster space should be at least several times larger than the  $10^7 M_{\odot}$  estimated above. As most of HII regions may still be in the halo, it is possible that star formation in stripped ISM is more efficient in the halo than in intracluster space. For the star clusters in the halo, some of them may remain bound, while others may escape the galactic potential through tidal interactions. Thus, this single transforming galaxy ESO 137-001 contributes over  $10^7 M_{\odot}$  of new stars in the halo and intracluster space through star formation in the ram-pressure displaced clouds, although it is unclear how many will end in intracluster space. If some large star clusters are bound to the galaxy for a significant amount of time, the configuration may look like galaxy aggregates found in the Coma cluster (Conselice & Gallagher 1998).

### 6.3. $H\alpha$ tail and stripping of the galactic ISM

There are not many cluster galaxies with known  $H\alpha$  tails, two irregular galaxies in the northwest of A1367 (Gavazzi et al. 2001), NGC 4388 in the Virgo cluster (Yoshida et al. 2002; 2004), a post-starburst galaxy near the center of the Coma cluster (Yagi et al. 2007), and several galaxies in an infalling compact group towards A1367 (Sakai et al. 2002; Gavazzi et al. 2003; Cortese et al. 2006). Both galaxies in the northwest of A1367 and the post-starburst galaxy in Coma have similar  $K_s$ -band absolute magnitudes as ESO 137-001's (from 0.49 mag fainter to 0.10 mag brighter), implying similar total stellar mass as ESO 137-001's. NGC 4388 is 1.3 mag more luminous than ESO 137-001 in the  $K_s$  band and also larger. Both  $H\alpha$  tails in A1367 are suggested to be produced by ram pressure stripping, while the tidal interaction between the two galaxies may trigger star formation in both galaxies (Gavazzi et al. 2001). The  $H\alpha$  tail behind the galaxy D100 in Coma is remarkably narrow and straight (60 kpc  $\times$  2 kpc). It may be produced through either ram pressure stripping, or comes from the gas of a merging dwarf (Yagi et al. 2007). The  $H\alpha$  filaments in the northeast of NGC 4388 are suggested to be ionized by NGC 4388's AGN, while ram pressure stripping of the ISM provides the cool gas trail (Yoshida et al. 2004). The remarkable infalling compact group in A1367 is composed of several giant galaxies, many dwarf galaxies and  $H\alpha$ -emitting knots. We notice that the *B* band absolute magnitude of the ELO1 (before correction on the intrinsic extinction) is comparable to the faint dwarf galaxies in



that infalling group ( $M_B = -15.3$  mag compared to  $-15.8$  mag). Cortese et al. (2006) suggested that the rich star formation phenomena in this infalling group is triggered by tidal interactions between group members and the ram pressure by the ICM. The galaxy C153 in A2125 ( $z=0.247$ ) is another similar case (Wang et al. 2004; Owen et al. 2006), with a wide 80 kpc [OII] tail that is also likely shown in the X-rays. The galaxy has a distorted disk with substantial star formation activity, just when it is penetrating the cluster core. However, it is far more distant than all other galaxies discussed here so the interaction cannot be studied in the same detail as others. There are no detections of X-ray tails behind the other galaxies with  $H\alpha$  tails in the *Chandra* or *XMM-Newton* data. There are also no reports of isolated HII regions near the two galaxies in the northwest of A1367 and D100 in Coma. The spectroscopically confirmed HII region by Gerhard et al. (2002) is north of NGC 4388 but is far away from the  $H\alpha$  filaments revealed by Yoshida et al. (2002). Other emission-line objects in that part of the Virgo cluster are even farther away from the  $H\alpha$  filaments (Fig. 1 of Okamura et al. 2002).

How does the  $H\alpha$  tail of ESO 137-001 form? The net  $H\alpha$  image of the galaxy shows the truncation of the  $H\alpha$  emission on the front and the sides (Fig. 1 and Fig. 6). In fact, the leading edge of the X-ray emission in ESO 137-001 coincides positionally with the  $H\alpha$  front. The compactness of the remaining  $H\alpha$  core demonstrates the strength of the ICM wind. Compared with simulations by Roediger & Hensler (2005), over 90% of the gas in the original gas disk should have been removed from the disk, either hanging up in the halo or in the tail. Thus, ram pressure stripping should play an important role in the formation of the observed  $H\alpha$  tail. The stellar ionization field in the tail may be too weak to ionize the stripped cold gas to produce the observed  $H\alpha$  tail, at least from the current data. The positional coincidence of the  $H\alpha$  tail and the X-ray tail implies a connection. Can heat conduction from the surrounding ICM to the cold stripped ISM provide enough energy? Heat conduction across the embedded cold clouds is most likely saturated. We use the saturated heat conductivity derived by Cowie & McKee (1977) to estimate the flow-in heat flux. The surface area is still estimated from a cylinder with a 3.5 kpc diameter and a 40 kpc length (§5), although the real contact surface is almost certainly higher (e.g., for clumpy clouds). The total heat luminosity is  $4.7 \times 10^{43}$  ergs  $s^{-1}$ , for an ICM temperature of 6.5 keV and an ICM density of  $10^{-3}$   $cm^3$ . Although the energy emitted through  $H\alpha$  is only a small fraction of the total optical line cooling (several percent from Voit, Donahue & Slavin 1994), there is enough heat energy for the observed  $H\alpha$  tail. However, heat conduction can be largely suppressed by magnetic field at the boundaries of the clouds. It is likely that both stripping and heat conduction contribute to the observed  $H\alpha$  tail. Spectroscopic studies of the  $H\alpha$  tail, though difficult, will better clarify its nature. Radio observations are also required to study the distribution of the cold atomic and molecular gas in and behind ESO 137-001.

## 7. CONCLUSIONS

ESO 137-001 is a star-forming galaxy with a dramatic X-ray tail (S06). In this work, we present optical imaging and spectroscopic data of ESO 137-001 from SOAR and the CTIO 1.5m telescopes. An  $H\alpha$  tail is found behind ESO 137-001, extending to at least 40 kpc from the galaxy. The  $H\alpha$  tail positionally coincides with the X-ray tail. We conclude that ram pressure stripping is responsible for the ISM tail, while heat conduction from the hot ICM may also contribute to the energy of the op-

tical lines. This discovery makes ESO 137-001 the only known cluster galaxy with an X-ray tail and an  $H\alpha$  tail. The  $H\alpha$  emission in ESO 137-001 is confined to the central  $\sim 1$  kpc (radius) region. The current nuclear SFR ( $\sim 1.2 M_\odot/yr$ ) and the largely enhanced stellar continuum (after correction of intrinsic extinction) around the center imply that a galactic bulge may be building up. At least 29 emission-line objects with high  $H\alpha$  flux are also revealed by the data. They all spatially cluster downstream of the galaxy, in or around the stripped ISM tail. Those closest to the galactic disk form a bow-like front. From analysis of the  $H\alpha_{off}$  frame and the estimate of the background emission-line objects, we conclude that the expected number of background objects is much less than one in the whole  $3.43' \times 3.88'$  field and all 29 emission-line objects are very likely HII regions associated with ESO 137-001. The high number density and luminosities of these HII regions downstream of ESO 137-001 dwarf the previously known examples of isolated HII regions in clusters, making ESO 137-001 a dramatic example full of rich phenomena. Interestingly, one *Chandra* point source (an ULX with  $L_X > 10^{40}$  ergs  $s^{-1}$  if in A3627) is in the same position as an HII region. All these detections indicate significant star formation activity in the halo of ESO 137-001 and in intracluster space.

Our data imply a connection between these HII regions and the stripping of the ISM. We suggest that star formation may proceed in the stripped ISM, in both the galactic halo and the intracluster space. The star formation in the halo may have a higher efficiency as the stripped ISM is still bound. Cooling can become dominant when the surrounding UV radiation field is much weaker than in the disk. Cloud collisions may also induce collapse of the ISM clouds. The total mass of the current starbursts in these 29 HII regions is about  $10^7 M_\odot$ . Since many HII regions and star clusters may have already faded, the total stellar mass formed in the stripped ISM may be several times higher. Therefore, stripping of the ISM not only contributes to the ICM, but also adds intracluster stellar light through subsequent star formation.

There is no reason to believe ESO 137-001 is unique. However, its current active stage may last only for a short time ( $< 10^8$  yr) so a large sample of cluster late-type galaxies has to be studied to find more similar ones like ESO 137-001, either in X-rays or  $H\alpha$ . Nevertheless, the proximity of ESO 137-001 makes it a good target to study galaxy transformation, the evolution of stripped ISM, star formation and X-ray binaries in the halo and the intracluster space, with the help of more data.

M. S. is very grateful to Allan Hornstrup, who made an early  $H\alpha$  observation using the Danish 1.54m telescope with observers Jan-Erik Ovaldsen, Josefine H. Selj, and Dong Xu. We thank Nathan De Lee for the help on the SOAR data analysis. We thank Fred Walter for the helps on the CTIO 1.5m data and the observation planning. We acknowledge the work of the SOAR operators Sergio Pizarro and Daniel Maturana, as well as the CTIO 1.5m service observers Alberto Miranda and Alberto Pasten. We thank the referee, Giuseppe Gavazzi, for helpful and prompt comments. The financial support for this work was provided by the NASA Grant AR6-7004X and NASA LTSA grant NNG-05GD82G. We are presenting data obtained with the Southern Observatory for Astrophysical Research, which is a joint project of the Brazilian Ministry of Science, the National Optical Observatories, the University of North Carolina and Michigan State University. We made use of the NASA/IPAC Extragalactic Database and the Hyperleda database.

## REFERENCES

- Bell, E. F., & De Jong, R. S. 2001, *ApJ*, 550, 212
- Bell, E. F., McIntosh, D. H., Katz, N., Weinberg, M. D. 2003, *ApJS*, 149, 289
- Butcher, H., & Oemler, A. Jr. 1984, *ApJ*, 285, 426
- Ciardullo, R., Jacoby, G. H., Feldmeier, J. J., Bartlett, R. E. 1998, *ApJ*, 492, 62
- Cardelli, J. A., Clayton, G. C., Mathis, J. S. 1989, *ApJ*, 345, 245
- Conselice, C. J., & Gallagher, J. S., III 1998, *MNRAS*, 297, L34
- Cortese, L. et al. 2004, *A&A*, 416, 119
- Cortese, L. et al. 2006, *A&A*, 453, 847
- Cortese, L. et al. 2007, *MNRAS*, 376, 157
- Cowie, L. L., McKee, C. F. 1977, *ApJ*, 211, 135
- Gavazzi, G. et al. 2001, *ApJ*, 563, L23
- Gavazzi, G. et al. 2003, *ApJ*, 597, 210
- Gavazzi, G. et al. 2006, *A&A*, 446, 839
- Gerhard, O. et al. 2002, *ApJ*, 580, L121
- Gnedin, O. Y. 2003, *ApJ*, 589, 752
- Gnedin, O. Y. et al. 2007, *ApJ*, in press, arXiv:astro-ph/0607394
- Gunn, J. E., & Gott, J. R., III 1972, *ApJ*, 176, 1
- Hamuy, M., Suntzeff, N. B., Heathcote, S. R., Walker, A. R., Gigoux, P., Phillips, M. M. 1994, *PASP*, 106, 566
- Leitherer, C. et al. 1999, *ApJS*, 123, 3
- Jarrett, T. H. 2000, *PASP*, 112, 1008
- Kennicutt, R. C., Jr. 1983, *ApJ*, 272, 54
- Kennicutt, R. C., Jr. 1998, *ARA&A*, 36, 189
- Kewley, L. J., & Dopita, M. A. 2002, *ApJS*, 142, 35
- Kewley, L. J., Groves, B., Kauffmann, G., Heckman, T. 2006, *MNRAS*, 372, 961
- Kraan-Korteweg, R. C., Woudt, P. A., Cayatte, V., Fairall, A. P., Balkowski, C., Henning, P. A. 1996, *Nature*, 379, 519
- Malhotra, S., Rhoads, J. E. 2002, *ApJ*, 565, L71
- Mendes de Oliveira, C., Cypriano, E. S., Sodr, L., Jr., & Balkowski, C. 2004, *ApJ*, 605, L17
- Merritt, D. 1988, in *ASP Conf. Ser. 5, The Minnesota Lectures on Clusters of Galaxies and Large-Scale Structure*, ed. J. Dickey (San Francisco: ASP), 175
- O'Connell, R. W. 2004, in *ASP Conf. Ser. 322, The Formation and Evolution of Massive Young Star Clusters*, ed. H. G. J. L. M. Lamers, L. J. Smith, & A. Nota (San Francisco: ASP), 551
- Okamura, S. et al. 2002, *PASJ*, 54, 883
- Oosterloo, T., Morganti, R., Sadler, E. M., Ferguson, A., van der Hulst, T., & Jerjen, H. 2004, in *IAU Symp. 217, Recycling Intergalactic and Interstellar Matter*, ed. P.-A. Duc, J. Braine, & E. Brinks (San Francisco: ASP), 486
- Oosterloo, T., & van Gorkom, J. 2005, *A&A*, 437, 19L
- Osterbrock, D. E. 1989, *Astrophysics of Gaseous Nebulae and Active Galactic Nuclei* (Mill Valley: University Science Books)
- Owen, F. N., Keel, W. C., Wang, Q. D., Ledlow, M. J., Morrison, G. E. 2006, *AJ*, 131, 1974
- Pascual, S. et al. 2001, *A&A*, 379, 798
- Quilis, V., Moore, B., & Bower, R. G. 2000, *Science*, 288, 1617
- Roediger, E., & Hensler, G. 2005, *A&A*, 433, 875 (RH05)
- Roediger, E., Brüggem, M., Hoeft, M. 2006, *MNRAS*, 371, 609
- Ryan-Weber, E. V. et al. 2004, *AJ*, 127, 1431
- Sakai, S., Kennicutt, R. C., Jr., van der Hulst, J. M., Moss, C. 2002, *ApJ*, 578, 842
- Schaye, J. 2004, *ApJ*, 609, 667
- Schulz, S., & Struck, C. 2001, *MNRAS*, 328, 185 (SS01)
- Sun, M., & Vikhlinin, A. 2005, *ApJ*, 621, 718
- Sun, M. et al. 2006, *ApJ*, 637, L81 (S06)
- Sun, M. et al. 2007, *ApJ*, 2007, 657, 197
- van Zee, L., et al. 1998, *AJ*, 116, 2805
- Voit, G. M., Donahue, M., Slavin, J. D. 1994, *ApJS*, 95, 87
- Vollmer, B., Cayatte, V., Balkowski, C., Duschl, W. J. 2001, *ApJ*, 561, 708
- Vollmer, B. et al. 2001, *A&A*, 369, 43
- Wang, Q. D., Owen, F., Ledlow, M. 2004, *ApJ*, 611, 821
- Woudt, P. A., Kraan-Korteweg, R. C., Fairall, A. P. 1999, *A&A*, 352, 39
- Woudt, P. A. et al. 2004, *A&A*, 415, 9
- Woudt, P. A., Kraan-Korteweg, R. C., Lucey, J., Fairall, A. P., Moore, S. A. W. 2007, *MNRAS*, submitted, arXiv:0706.2227
- Yagi, M. et al. 2007, *ApJ*, 660, 1209
- Yoshida, M. et al. 2002, *ApJ*, 567, 118
- Yoshida, M. et al. 2004, *AJ*, 127, 90

TABLE 1  
 PROPERTIES OF REPRESENTATIVE EMISSION-LINE OBJECTS (PUTATIVE HII REGIONS)

ID <sup>a</sup>	$L_{H\alpha}$ <sup>b</sup> ( $10^{39}$ ergs s <sup>-1</sup> )	$Q(H^0)$ <sup>c</sup> ( $10^{51}$ s <sup>-1</sup> )	$M_B$ <sup>d</sup> (mag)	$M_I$ <sup>d</sup> (mag)	EW (H $\alpha$ ) <sup>e</sup> ( $\text{\AA}$ )	Age <sup>f</sup> (Myr)	Mass <sup>g</sup> ( $10^5 M_\odot$ )	N(O) <sup>h</sup> ( $10^2$ )
1	21	21	-15.29	-16.76	138	3.4, 5.4, 6.0, 6.0	38	89
2	8.6	8.5	-13.62	-13.82	614	2.7, 3.2, 4.7, 4.7	5.3	20
3	6.8	6.6	-13.32	-13.92	437	2.6, 3.5, 4.8, 4.8	5.9	21
4	1.4	1.4	-13.39	-14.17	68	5.0, 5.7, 6.7, 6.5	4.6	7.7
5	1.0	0.99	-12.00	-12.42	281	3.4, 4.7, 5.1, 5.0	0.95	3.4
6	0.096	0.095	>-10.48	>-11.02	>90	<5.0, <5.4, <6.3, 3.0	0.019	0.07
7	1.3	1.3	-11.28	>-11.94	>320	2.3, <3.4, <5.0, 3.5	0.43	1.9
8	0.10	0.10	>-10.59	>-11.14	>95	<5.0, <5.5, <6.3, 5.0	0.096	0.34

<sup>a</sup>Source ID (see Fig. 1c and 1d)

<sup>b</sup>1 mag intrinsic extinction assumed (see §3.3 for more detail)

<sup>c</sup>The number of H-ionizing photons estimated from  $L_{H\alpha}$

<sup>d</sup>Absolute magnitudes without correction on intrinsic extinction

<sup>e</sup>The equivalent width of H $\alpha$  line assuming an [NII] fraction of 19% (see §3.3)

<sup>f</sup>The age of the current starburst estimated from Starburst99 (see §3.3). The first three values are estimated from  $Q(H^0)/L_B$ ,  $Q(H^0)/L_I$  and EW (H $\alpha$ ), while the final value is the chosen age to estimate the next two properties. We generally use the age derived from EW (H $\alpha$ ) if it is well determined, as EW (H $\alpha$ ) is not affected by intrinsic extinction. Different ages for similar objects #6 and #8 are chosen to demonstrate the change of the total mass and the number of O stars with the choice of the starburst age.

<sup>g</sup>The total mass in the instantaneous starburst estimated from Starburst99

<sup>h</sup>The number of O stars estimated from Starburst99

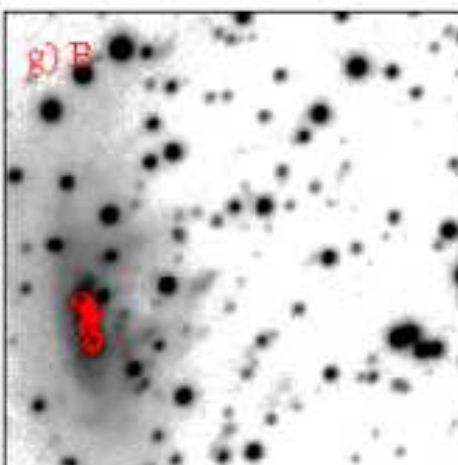
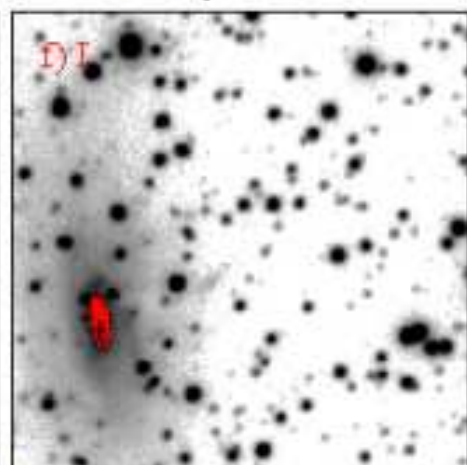
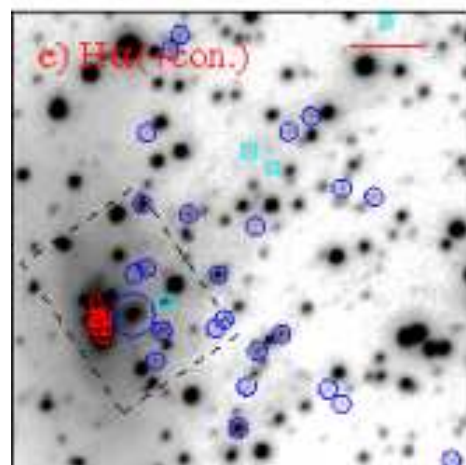
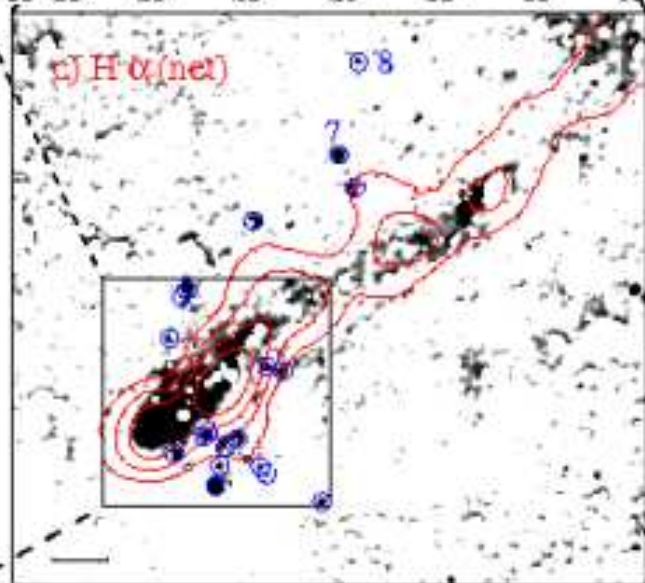
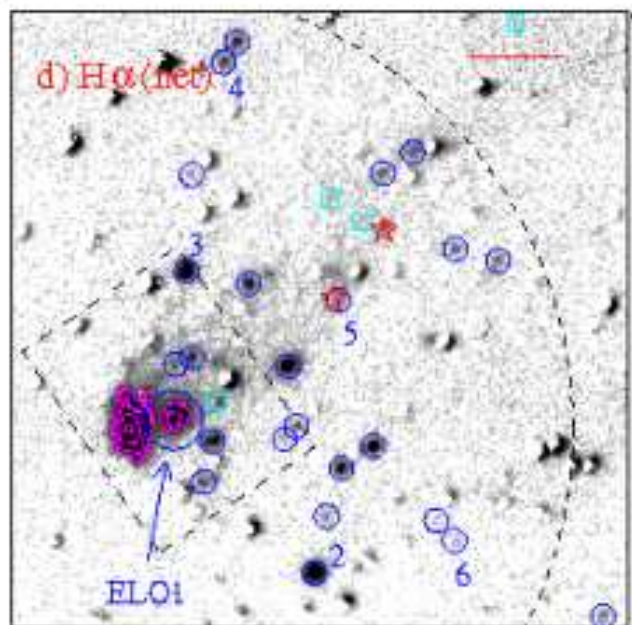
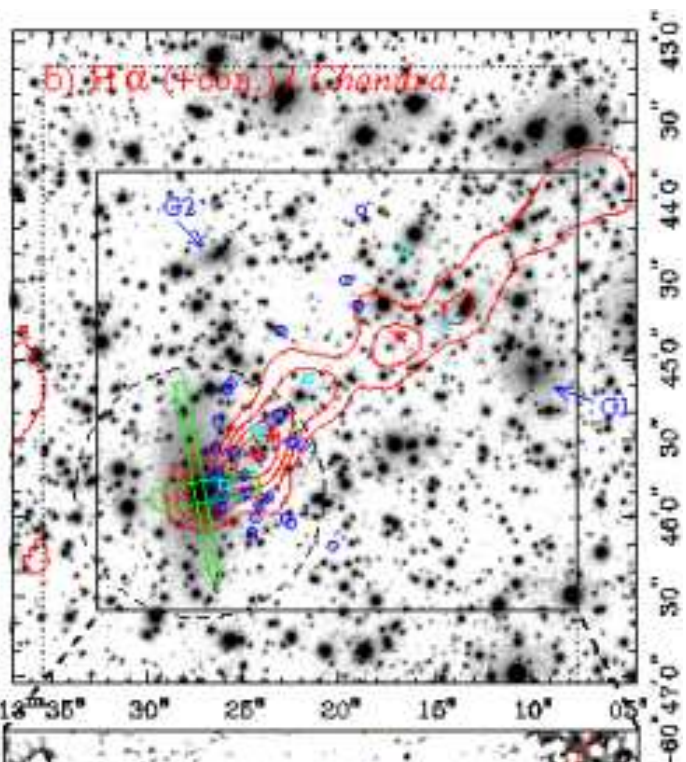
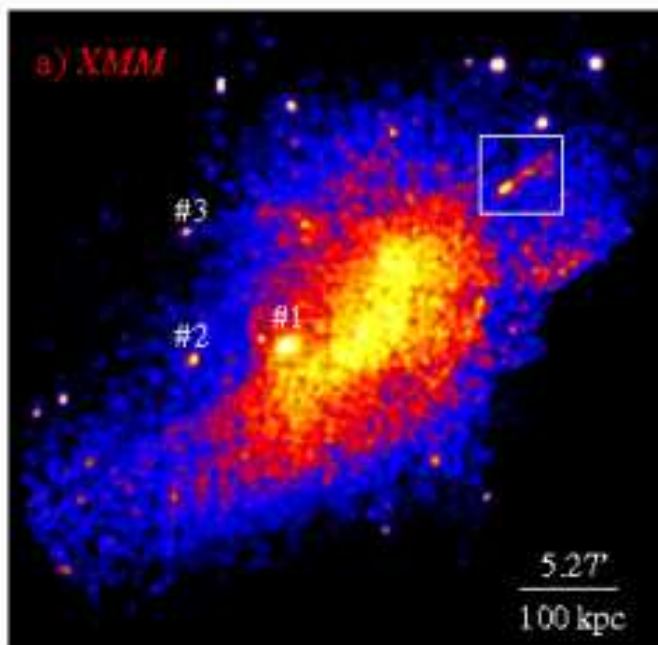


FIG. 1. — **a**): XMM-Newton 0.5 - 2 keV mosaic of A3627 (background-subtracted and exposure corrected). A long X-ray tail is significant as shown in the white box. The brightest three cluster galaxies (in the  $K_s$  band) are away from the cluster gas core (ESO 137-006 - #1, ESO 137-008 - #2 and ESO 137-010 - #3). **b**): the zoom-in of the region around ESO 137-001's tail ( $4.0' \times 4.1'$ ). *Chandra* contours (from the 0.5 - 2 keV smoothed image, in red) are superposed on the  $H\alpha$  (+ continuum) image. The dotted box region is where data in  $H\alpha$ ,  $H\alpha_{\text{off}}$ ,  $B$  and  $I$  bands are all available and colors are measured in Fig. 2. Three *Chandra* point sources in the tail are also marked as red stars. Blue circles mark emission-line objects selected from colors in Fig. 2, while cyan boxes mark six more sources selected if criteria to select emission-line objects are relaxed (§3.1). The green rectangles mark the regions where surface brightness profiles are measured along the minor and major axes shown in Fig. 6. The dashed-line circle (15 kpc in radius) shows the approximate size of the tidally truncated dark matter halo of ESO 137-001 (also in d). Most of the emission-line objects may still be in the halo, but the most distant three are 29 - 39 kpc from the nucleus. G1 and G2 are the only two galaxies within 100 kpc from the end of ESO 137-001's X-ray tail (velocity unknown). The cluster is close to the Galactic plane (Gal. latitude of -7 deg) so the foreground star density is high. **c**): net  $H\alpha$  emission (smoothed) in a contrast to enhance the emission from the diffuse tail, superposed on the *Chandra* contours (red). Stars are masked. Beyond the  $H\alpha$  tail and the emission-line objects (in blue circles for those outside the tail), the residual emission is generally around bright stars. The scale bar is 5 kpc (or  $15.8''$ ). The X-ray leading edge in the current short *Chandra* exposure is actually around the same position as the  $H\alpha$  edge, as the shown *Chandra* contours are from a smoothed image. **d**): net  $H\alpha$  emission in the galaxy and the head of the tail ( $1.1' \times 1.1'$ ). The contours (in magenta) around the peaks are also shown. Symbols have the same meaning as in b). Eight representative emission-line objects are marked from ELO1 to 8 (sources 7 and 8 in panel c). The box is the aperture used to measure the total net  $H\alpha$  flux from the galaxy (§4). The scale bar is  $10''$  (or 3.17 kpc). **e**):  $H\alpha$  (+ continuum) image of the same region as d). The nuclear region is also shown in red contours (similar in the next two panels). The scale bar is  $10''$ . **f**):  $I$  band image in the same field as d). **g**):  $B$  band image in the same field as d). Two blue features (from the  $B - I$  image) downstream of the galaxy are shown by arrows. There are also broad-band features to the south of ELO1.

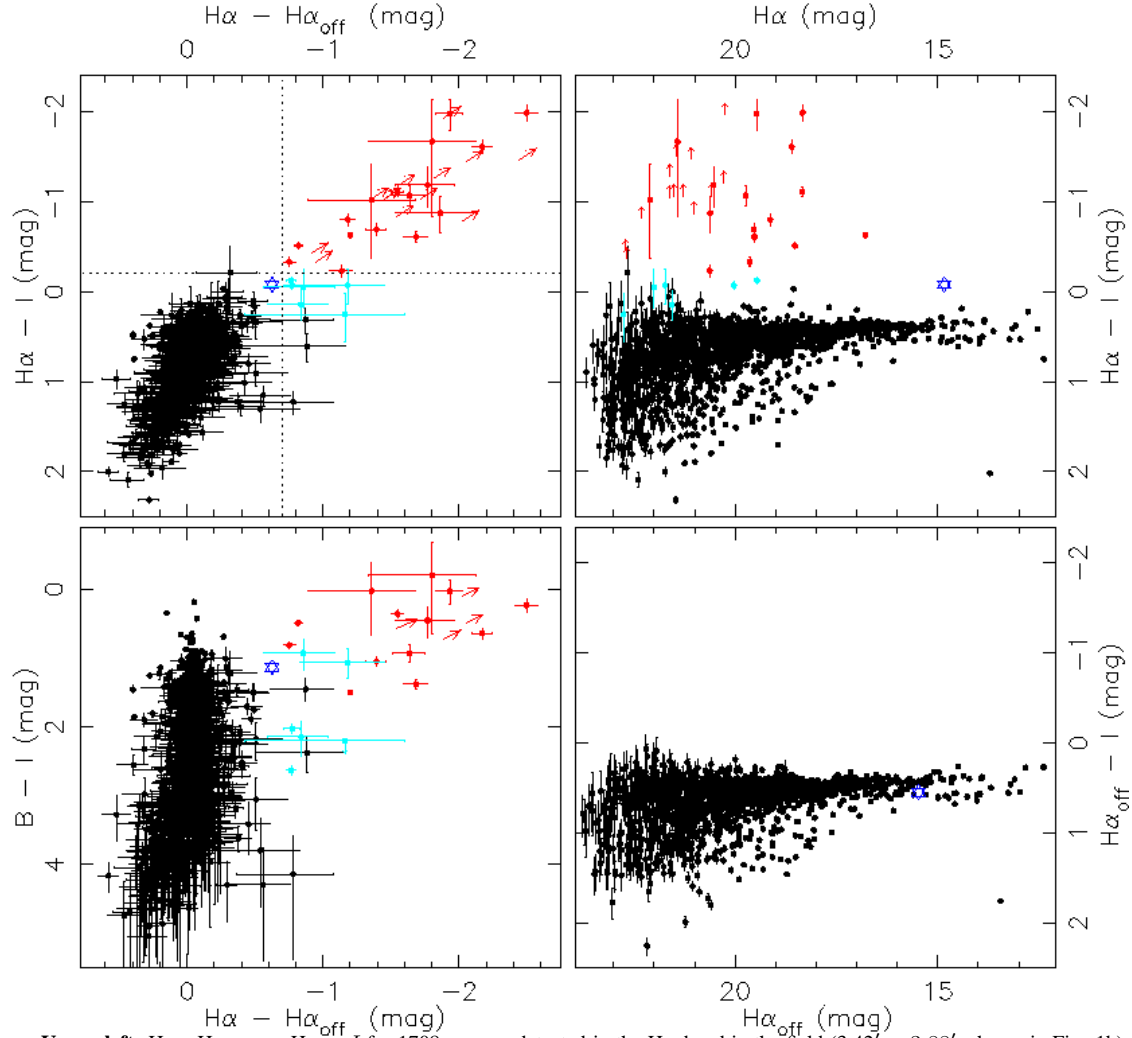


FIG. 2.— **Upper left:**  $H\alpha - H\alpha_{\text{off}}$  vs.  $H\alpha - I$  for 1708 sources detected in the  $H\alpha$  band in the field ( $3.42' \times 3.88'$ , shown in Fig. 1b). Both the  $H\alpha$  and the  $H\alpha_{\text{off}}$  fluxes include continuum. Over 97% of them are Galactic stars with  $H\alpha - H\alpha_{\text{off}}$  color close to zero. We define 29 emission-line objects (in red) as sources with  $H\alpha - I < -0.2$  mag and  $H\alpha - H\alpha_{\text{off}} < -0.7$  mag (dotted lines). The  $H\alpha$  and  $H\alpha_{\text{off}}$  magnitudes are AB magnitudes (Hamuy et al. 1994). We have corrected the Galactic extinction for all sources (including Galactic stars, 0.15 mag reddening for the  $H\alpha - I$  color) but no correction on the intrinsic extinction associated with ESO 137-001 has been applied (also the case for the next three plots). The blue star marks the position of ESO 137-001's central region where the giant  $H\alpha$  nebula is, measured within a  $3'' \times 6''$  (semi-axes) ellipse centered on the  $H\alpha$  peak (also in the next three plots). If we relax the selection criteria (see §3.1), six more candidate emission-line objects are selected (in cyan). **Upper right:**  $H\alpha$  magnitude vs.  $H\alpha - I$  color. **Lower left:**  $H\alpha - H\alpha_{\text{off}}$  color vs.  $B - I$  color for sources where the  $B - I$  color can be constrained. The emission-line objects appear blue and most of them are bluer than ESO 137-001's core (no correction on the intrinsic extinction). The Galactic reddening for the  $B - I$  color (0.49 mag) has been applied to all sources. With a small amount of intrinsic extinction, the  $B - I$  colors of emission-line objects are close to that for pure O/B stars (-0.2 to -0.8 mag). **Lower right:**  $H\alpha_{\text{off}}$  magnitude vs.  $H\alpha_{\text{off}} - I$  color for sources detected in the  $H\alpha_{\text{off}}$  band. There are no emission-line objects detected in the  $H\alpha_{\text{off}}$  band with  $H\alpha_{\text{off}} - I < -0.2$  mag. Moreover, no objects are detected with  $H\alpha_{\text{off}} - H\alpha < -0.5$  mag and  $H\alpha_{\text{off}} - I < 0.25$  mag.

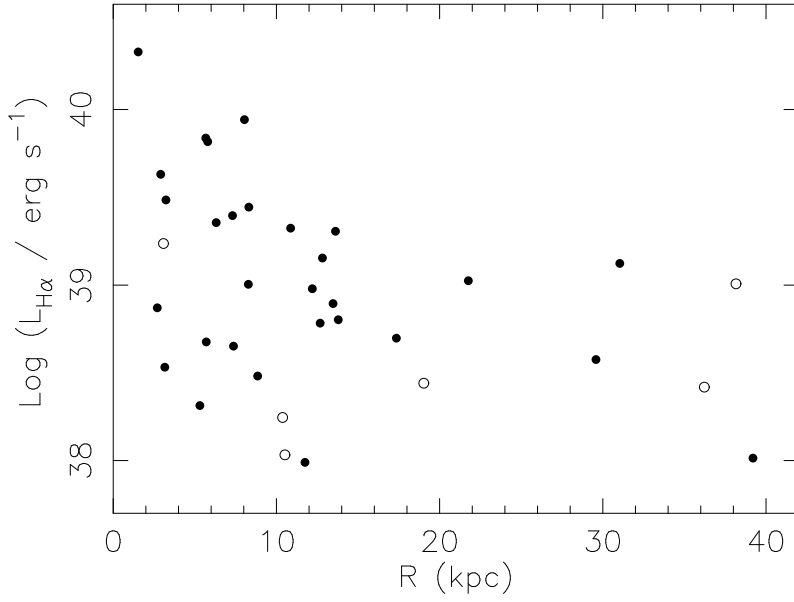


FIG. 3.— The luminosities of HII regions plotted with their distances to ESO 137-001’s nucleus. The data points in empty circles are six additional sources if the criteria for emission-line objects are relaxed (§4). We assumed 1 mag of intrinsic extinction for all of them. For comparison, the two isolated HII regions in the Virgo cluster (Gerhard et al. 2002; Cortese et al. 2004) have H $\alpha$  luminosities of  $1.3 \times 10^{37}$  ergs s<sup>-1</sup> and  $2.9 \times 10^{38}$  ergs s<sup>-1</sup> respectively (intrinsic extinction corrected).



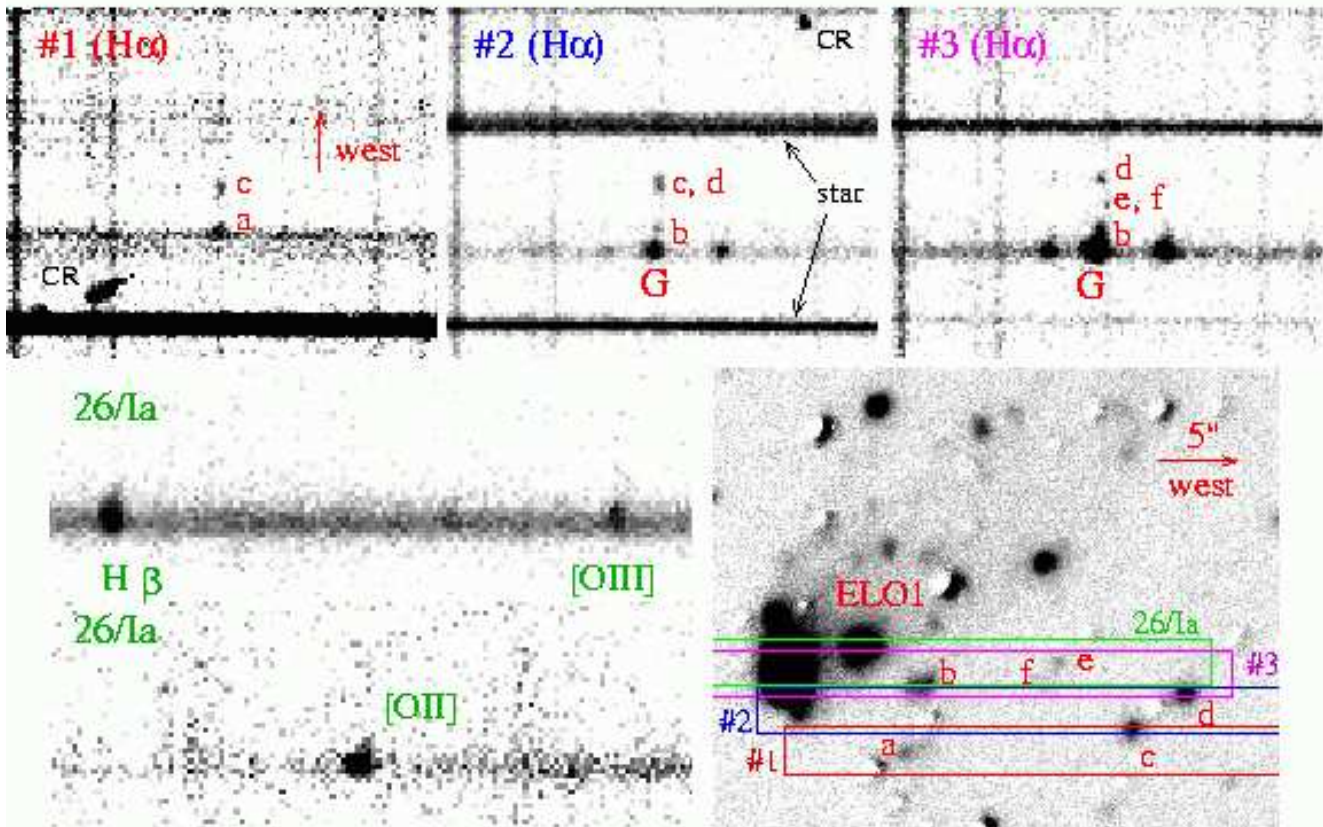


FIG. 4.— The long-slit spectra from the three 47/Ib slit positions and the 26/Ia slit position (in two wavelength ranges) shown in the upper panels and the lower left panel, while these four slit positions are shown on the net  $H\alpha$  image (the lower right panel). The dispersion axis is always horizontal and the spatial axis is always perpendicular on the detector plane (the west is upward). Note that each slit has a length of  $\sim 5''$  and a width of  $3''$  centered on the galaxy, while the slits plotted are truncated only for better viewing. The three 47/Ib 2D spectra are spatially aligned. The #1 position completely misses the  $H\alpha$  emission of the galaxy, while the #3 position covers the  $H\alpha$  peak of the galaxy. Emission-line objects (ELO1, and a - f as marked) were caught in one or more slit positions as shown in the spectra. The small scale-bar in the #3 plot (near “G”) is  $6.56\text{\AA}$ , or  $300\text{ km/s}$ . The slit for the 26/Ia observation runs across the peak of the galaxy and a large part of ELO1. The 26/Ia spectrum shows extension to the direction of ELO1 (upward on the detector plane) for the three strong lines, which implies that ELO1 has nearly the same velocity as ESO 137-001’s. Note that the best instrumental spatial seeing for the spectrograph is  $3.5''$  (or 2.7 pixels).

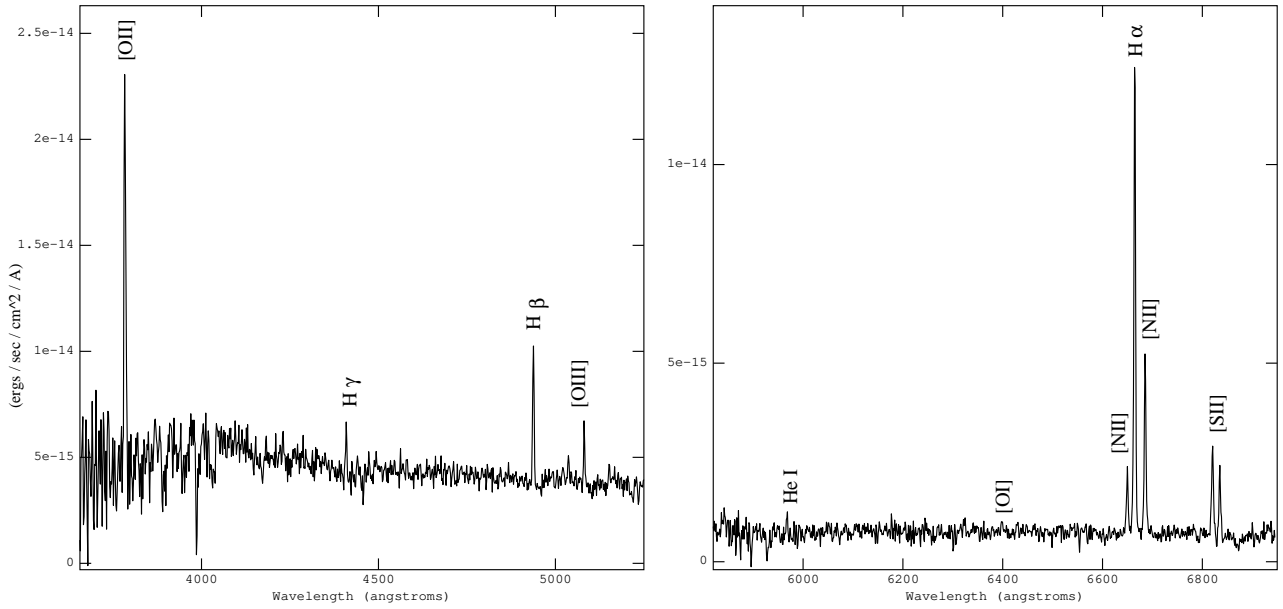


FIG. 5.— The CTIO 1.5m spectra of ESO 137-001’s core in two wavelength ranges. The  $H\alpha$  spectrum was taken at the slit position #3 (Fig. 4). Emission lines are marked. The line widths are all small (e.g.,  $3.7 \text{ \AA}$  FWHM for the  $H\alpha$  line). As the spectroscopic standards were observed with  $2''$  slits, the shown flux of each spectrum is over-estimated by an unknown constant, but the spectral shape and line ratios are not affected.

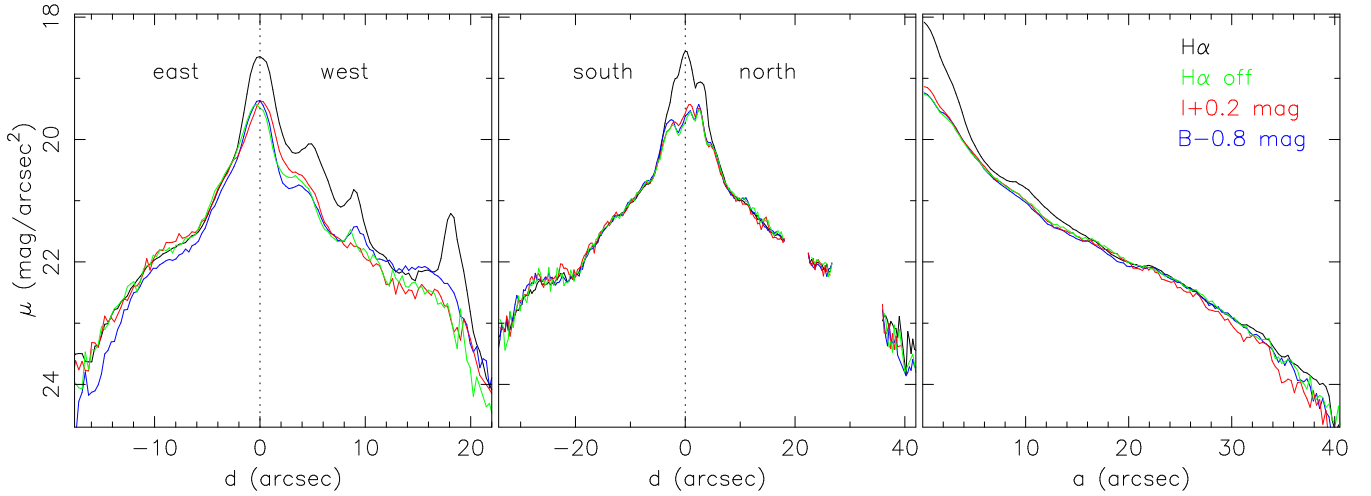


FIG. 6.— **Left:** Surface brightness profiles measured parallel to the minor axis of the galaxy (shown as a green box in Fig. 1b,  $8''$  width) in four bands (color coding in the right plot). We chose the origin as the peak of the  $H\alpha$  profile (same in the next two plots). Stars are masked but emission-line objects are included (also for the plot shown in the middle panel). The  $H\alpha_{\text{off}}$  light traces the  $H\alpha$  light well upstream (or east) until  $\sim 3''$  (or  $\sim 0.9 \text{ kpc}$ ) from the  $H\alpha$  peak. The three  $H\alpha$  peaks downstream are emission-line objects. The enhanced  $B$  band light downstream (relative to  $I$  band) is related to the emission-line objects. The  $I$  band profile at  $-15'' - -5''$  can be fitted with an exponential profile with a scale height of  $\sim 6.0''$ . **Middle:** Surface brightness profiles measured parallel to the major axis of the galaxy (shown as a green box in Fig. 1b,  $4''$  width) in four bands. The  $H\alpha_{\text{off}}$  light and the scaled continuum light trace the  $H\alpha$  light well beyond the central  $5''$  (or  $\sim 1.6 \text{ kpc}$ ). The continuum light within the central  $5''$  is flattened with substructures (also shown in Fig. 1e and 1f). Surface brightness of some area in the north is absent because of bright stars there. If the profiles at  $-26'' - -6''$  and  $9'' - 37''$  are fitted with exponential profiles respectively, the derived scale heights are  $\sim 11.9''$  in the south and  $\sim 13.3''$  in the north. **Right:** Surface brightness profiles measured in elliptical annuli are plotted against the semi-major axis ( $a$ ). The elliptical annuli are centered on the  $H\alpha$  peak of the galaxy and have a fixed axis ratio of 2 ( $a/b$ ,  $b$ : semi-minor axis). The positional angle is the same as that used to measure the surface brightness profiles along the major axis in the middle panel (Fig. 1b). All unresolved sources (including all emission-line objects but ELO1) are masked. The  $B$  and  $I$  profiles at  $7'' - 32''$  can be well fitted with an exponential profile with a scale height of  $\sim 9.5''$  (or  $3 \text{ kpc}$ ).